Dihydrogen Thiolate vs Hydride Thiol: Reactivity of the Series of Complexes $MH(CO)(L)(PPh_3)_2$ (M = Ru, Os; L = Pyridine-2-thiolate, Quinoline-8-thiolate) with Acid. X-ray Structure Determination of $[Os(CO)(\mu_2\text{-Spy})(SpyH)(PPh_3)]_2[BF_4]_2$

Marcel Schlaf, Alan J. Lough, and Robert H. Morris*

Lash Miller Chemical Laboratories, Department of Chemistry, University of Toronto, Toronto, Ontario M5S 3H6, Canada

Received May 28, 1996[⊗]

The complexes $MH(CO)(quS)(PPh_3)_2$ (M = Ru, Os; quS = quinoline-8-thiolate) are synthesized in a manner analogous to that for the known complexes $MH(CO)(pyS)(PPh_3)_2$ (M = Ru, Os; pyS = pyridine-2-thiolate). The isomer distribution in the quinoline-8-thiolate complexes was determined by an nOe experiment. It is inverted relative to the pyridine-2-thiolate complexes. EHMO calculations on the free chelate anions and the complexes $OsH(CO)(L)(PPh_3)_2$ (L = pyridine-2-thiol, quinoline-8-thiol) qualitatively show this to be a consequence of the different electronic properties of the chelate ligand. The electrochemistry of the complexes has been investigated. Protonation of the complexes with HBF_4 at low temperature results in the formation of mixtures of dihydrogen complexes $[M(\eta^2\text{-}H_2)(CO)(L)(PPh_3)_2]BF_4$ (M = Ru, Os; L = pyridine-2-thiolate, quinoline-8-thiolate) and thiol hydride complexes $[MH(CO)(LH)(PPh_3)_2]BF_4$ (M = Ru, Os; LH = pyridine-2-thiol, quinoline-8-thiol) in varying tautomer ratios. The structure of the thiol hydride complexes was determined using a heteronuclear decoupling $^1H\{^{31}P\}$ experiment. At low temperature the complexes $[Os(\eta^2\text{-}H_2)(CO)(quS)(PPh_3)_2]^+$ and $[Os(H)(CO)(quSH)(PPh_3)_2]^+$ are in tautomeric equilibrium. The influence of the chelate and the metal on the relative acidity and stability of the protonated complexes is discussed. The order of acidity of the complexes $[M(\eta^2\text{-}H_2)(CO)(L)(PPh_3)_2]BF_4$ is Os > Ru and pyS^- > quS^-. The majority of the complexes are thermally unstable with respect to loss of dihydrogen gas and/or decomposition. The single-crystal X-ray structure of the dimeric complex $[Os(CO)(\mu_2\text{-Spy})(SpyH)(PPh_3)]_2[BF_4]_2$, a nonstoichiometric decomposition product of the dihydrogen complex $[Os(\eta^2\text{-}H_2)(CO)(pyS)(PPh_3)_2]BF_4$, is presented. It contains a monodentate mercaptopyridinium ligand (SpyH) and face-to-face pyridyl rings, a structural motif which is becoming common for the $\mu_2\text{-}Spy^-$ ligand.

Introduction

The protonation of metal hydride complexes is a general route to the formation of dihydrogen complexes.[1] If the resulting dihydrogen complex is relatively electron poor and activates the $\eta^2\text{-}H_2$ ligand heterolytically, it can act as a strong inter- or intramolecular acid.[2,3] In the latter case, there is the possibility of selective proton transfer to a basic ancillary ligand to produce the hydride tautomer M(H)(LH) and/or a tautomeric equilibrium between the hydride and dihydrogen tautomers (eq 1).

$$M(\eta^2\text{-}H_2)(L) \rightleftarrows M(H)(HL) \qquad (1)$$

Such a tautomeric equilibrium could be observed by NMR, if the relative acidities of the dihydrogen ligand and the protonated ancillary ligand are not more than 2 pK_a units apart. This type of proton transfer or equilibrium might be a step in the mechanism of hydrogenase[4−6] and may also be responsible for the evolution of hydrogen gas from nitrogenase.[7] In industrial processes it might occur on the surface of Cu/ZnO catalysts in the synthesis of methanol and in hydroformylation reactions with homogeneous cobalt or rhodium catalysts.[8,9] Albéniz et al. have shown that the complex $OsH(\eta^2\text{-}S_2CH)(CO)(PiPr_3)_2$ reacts with acid to give, depending on the solvent, either the dihydrogen complex $[Os(\eta^2\text{-}H)_2(\eta^2\text{-}S_2CH)(CO)(PiPr_3)_2]^+$ or the methanedithiolate complex $[OsH(\eta^2\text{-}S_2CH_2)(CO)(PiPr_3)_2]^+$, but no equilibrium between the two tautomers as in eq 1 was observed.[10] We recently presented the first example of the direct observation of an equilibrium (eq 1) between the two tautomeric complexes $[Os(\eta^2\text{-}H_2)(CO)(quS)(PPh_3)_2]BF_4$ and $[Os(H)(CO)(quSH)(PPh_3)_2]$-

[⊗] Abstract published in *Advance ACS Abstracts,* September 1, 1996.

(1) Jessop, P. G.; Morris, R. H. *Coord. Chem. Rev.* **1992**, *121,* 155−284.
(2) Jia, G.; Morris, R. H.; Schweitzer, C. T. *Inorg. Chem.* **1991**, *30,* 593−594.
(3) Schlaf, M.; Morris, R. H. *J. Chem. Soc., Chem. Commun.* **1995**, 625−626.
(4) Crabtree, R. H. *Inorg. Chim. Acta* **1986**, *125,* L7−L8.
(5) Hembre, R. T.; McQueen, S. *J. Am. Chem. Soc.* **1994**, *116,* 2141−2142.
(6) Efros, L. L.; Thorp, H. H.; Brudvig, G. W.; Crabtree, R. H. *Inorg. Chem.* **1992**, *31,* 1722−1724.
(7) Lowe, D. J.; Fisher, K.; Thorneley, R. N. F. *Biochem. J.* **1990**, *272,* 621−625.
(8) Versluis, L.; Ziegler, T. *Organometallics* **1990**, *9,* 2985−2992.
(9) Pino, P.; Major, A.; Spindler, F.; Tannenbaum, R.; Bor, G.; Horvath, I. T. *J. Organomet. Chem.* **1991**, *417,* 65−76.
(10) Albéniz, M. J.; Buil, M. L.; Esteruelas, M. A.; López, A. M.; Oro, L. A.; Zeier, B. *Organometallics* **1994**, *13,* 3746−3748.

S0276-7333(96)00411-6 CCC: $12.00

Table 1. List of Observed Compounds and Numbering Scheme

complex	H *trans* to N	H *trans* to S
$RuH(CO)(pyS)(PPh_3)_2$	**1a**	**1b**
$OsH(CO)(pyS)(PPh_3)_2$	**2a**	**2b**
$RuH(CO)(quS)(PPh_3)_2$	**3a**	**3b**
$OsH(CO)(quS)(PPh_3)_2$	**4a**	**4b**
$[Ru(\eta^2\text{-}H_2)(CO)(pyS)(PPh_3)_2]BF_4$	**5a**	**5b**
$[RuH(CO)(pySH)(PPh_3)_2]BF_4$	**5c**	*a*
$[Os(\eta^2\text{-}H_2)(CO)(pyS)(PPh_3)_2]BF_4$	**6a**[a]	**6b**[a]
$[Ru(\eta^2\text{-}H_2)(CO)(quS)(PPh_3)_2]BF_4$	**7a**	**7b**
$[RuH(CO)(quSH)(PPh_3)_2]BF_4$	**7c**	**7d**
$[Os(\eta^2\text{-}H_2)(CO)(quS)(PPh_3)_2]BF_4$	**8a**	**8b**
$[OsH(CO)(quSH)(PPh_3)_2]BF_4$	**8c**	**8d**

[a] **5d** and **6c**,**d** are not observed.

BF_4 (quSH = quinoline-8-thiol).[3] We also reported the structure and reactivity of the complex $[Os(\eta^2\text{-}H_2)(CO)(pyS)(PPh_3)_2]BF_4$ (pyS^- = pyridine-2-thiolate), one of the most acidic yet stable dihydrogen complexes known to date.[11] Here we present the results of the protonation of the complete series of complexes $MH(CO)(L)(PPh_3)_2$ (M = Ru, Os; L = pyS^-, quS^-), leading to the series of tautomeric complexes $[M(\eta^2\text{-}H_2)(CO)(L)(PPh_3)_2]BF_4$ and $[MH(CO)(LH)(PPh_3)_2]BF_4$.

Results

All observed protonated and parent monohydride complexes with their numbering schemes throughout this paper are listed in Table 1.

Synthesis of $MH(CO)(quS)(PPh_3)_2$ (M = Ru, Os). The complexes $MH(CO)(quS)(PPh_3)_2$ (M = Ru (**3**), Os (**4**)) were synthesized by use of a method analogous to the synthesis of the pyridine-2-thiolate complexes $MH(CO)(pyS)(PPh_3)_2$ (M = Ru (**1**), Os (**2**)) described by Robinson and Mura.[12,13] Complexes **3** and **4** are obtained respectively as 1:3 and 1:2 isomeric mixtures of isomers **a** and **b** by refluxing a mixture of $MH_2(CO)(PPh_3)_3$ with a slight excess of quinoline-8-thiol in toluene (eq 2).

$$MH_2(CO)(PPh_3)_3 + quSH \rightarrow MH(CO)(quS)(PPh_3)_2 + PPh_3 + H_2 \quad (2)$$

The oxygen-sensitive quinoline-8-thiol is prepared from the commercially available quinoline-8-thiol hydrochloride.[14] The preparation of **3** can be simplified by reacting the starting material with quinoline-8-thiol hydrochloride in a biphasic mixture of water and toluene, in which the hydrochloride is deprotonated *in situ* with an excess of $NaHCO_3$. The resulting free thiol is immediately taken up by the organic phase. This procedure fails in the preparation of **4**. The reaction of $OsH_2(CO)(PPh_3)_3$ with quinoline-8-thiol hydrochloride does not proceed in the biphasic mixture but requires the higher reaction temperatures achieved by refluxing in pure toluene containing the water-insoluble thiol. The monohydride complexes are deep red (**3**) or purple (**4**) air-stable solids soluble in CH_2Cl_2, $CHCl_3$, or toluene. Attempts to separate the isomers by fractional crystallization were unsuccessful. Only samples enriched in the minor isomer **a** were obtained.

Table 2. NMR and IR Spectroscopic Properties and Isomer Percentages of Complexes $MH(CO)(L)(PPh_3)_3$ (1−4)

	yield (%)	δ(MH) (ppm)[b]	$^2J_{HP}$ (Hz)	δ(H-*o*-N)[a] (ppm)[b]	δ(PPh_3) (ppm)[c]	ν(CO) (cm^{-1})[d]
1a[e]	85	−12.30 (t)	20.3	6.18 (d)	48.9 (s)	1905
1b[e]	15	−11.55 (t)	20.0	*f*	50.3 (s)	1909
2a[e]	85	−13.91 (t)	17.6	6.10 (d)	21.3 (s)	1888
2b[d,e]	15	−12.34 (t)	19.7	*f*	22.6 (s)	1894
3a	25	−11.53 (t)	19.7	8.58 (d)	45.9 (s)	1921
3b	75	−8.65 (t)	18.7	8.40(d)	47.9(s)	1945
4a	30	−12.71 (t)	18.2	8.59 (d)	17.8 (s)	1903
4b	70	−9.54 (t)	17.3	8.42 (d)	19.8 (s)	1923

[a] Proton *ortho* to nitrogen in chelate ring. [b] $CDCl_3$. [c] Toluene (relative to 85% H_3PO_4). [d] CH_2Cl_2. [e] Cf. refs 12 and 13. [f] Signal obscured by peaks of major isomer.

Isomer Assignments and Spectroscopic Properties of the Monohydride Complexes 1−4. The spectroscopic properties of compounds **1**−**4** are summarized in Table 2. The ^{31}P NMR spectra of the complexes **1**−**4** in toluene each show two singlets between 17 and 51 ppm for the two isomers. The signals for the osmium complexes **2**[12] and **4** are both shifted approximately 27 ppm upfield from those of the ruthenium complexes **1**[12] and **3**. The signals for the hydride ligands appear as 1:2:1 triplets between −8 and −14 ppm in $CDCl_3$ with coupling constants of 17.3−20.3 Hz. Identification of the resonances of the protons *ortho* to the nitrogen atom of the chelate is important for the absolute isomer assignment of the quinoline-8-thiolate complexes by nOe experiments (*vide infra*). In the spectra of the quinoline-8-thiolate complexes **3a,b** and **4a,b** the protons *ortho* to the nitrogen atom appear above 8 ppm, distinctively offset from other signals as is normally observed for quinolines and pyridines.[15,16] In the pyridine-2-thiol complexes the chemical shifts of the protons *ortho* to the nitrogen atom are strongly affected by coordination to the metal and no longer appear above 8 ppm. We tentatively assign the most downfield doublets at 6.18 and 6.10 ppm to the protons *ortho* to the nitrogen atom in the pyridine-2-thiolate complexes **1a** and **2a**, respectively. For the complexes **1** and **2**, the major isomer is **a** in which the hydride ligand is *trans* to the nitrogen atom of the chelate. This isomer assignment is based on a single-crystal X-ray structure analysis of the corresponding dihydrogen complex **6a**[11] and is opposite to the one suggested by Mura et al.[12] For the complexes **3** and **4** the major isomer is **b**, in which the hydride ligand is *trans* to the sulfur atom of the chelate. This isomer assignment is based on an nOe difference experiment carried out on the isomeric mixtures of **3** and **4**. Figure 1 illustrates the stereochemical differences in the two isomers and the approach taken in the nOe experiment. Selective irradiation of the smaller hydride signal of the isomeric mixture of **3** does not result in any detectable nOe on the corresponding *ortho* proton signal of that isomer at 8.58 ppm, whereas irradiation of the larger hydride signal leads to an expressed nOe of 16% on the corresponding *ortho* proton signal of that isomer at 8.40 ppm.

(11) Schlaf, M.; Lough, A. J.; Morris, R. H. *Organometallics* **1993**, *12*, 3808−3809.
(12) Mura, P.; Olby, B. G.; Robinson, S. D. *J. Chem. Soc., Dalton Trans.* **1985**, 2101−2112.
(13) Alteparmakian, V.; Mura, P.; Olby, B. G.; Robinson, S. D. *Inorg. Chim. Acta* **1985**, *104*, L5.
(14) Edinger, A. *Chem. Ber.* **1908**, *41*, 937−943.
(15) Simons, W. W. *The Sadtler Handbook of Proton NMR Spectra*; Sadtler Research Laboratories: Philadelphia, PA, 1978.
(16) Hesse, M.; Meier, H.; Zeh, B. *Spektroskopische Methoden in der Organischen Chemie*; Georg Thieme Verlag: Stuttgart, 1987.

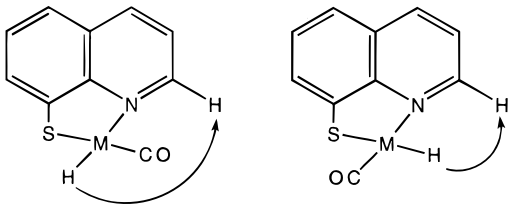

Figure 1. Isomers of **3** and **4** with observed nOe's. The PPh_3 ligands above and below the paper plane are omitted for clarity.

The analogous experiment with **4** results in a signal enhancement of 19% on the larger *ortho* proton signal at 8.42 ppm of the isomer mixture. From this we conclude that the major isomers are **b** with the hydride ligand *trans* to the sulfur atom of the chelate.

The change of pyridine-2-thiolate in **1** and **2** to quinoline-8-thiolate in **3** and **4** as the chelating ligand therefore leads to an inversion of the isomer distribution. The established isomer assignments are consistent with several trends in the spectroscopic data listed in Table 2. In all cases the hydride signal of the isomer in which the hydride ligand is *trans* to the nitrogen atom of the chelate (isomer **a**) appears at higher field than that in which the hydride ligand is *trans* to the sulfur atom (isomer **b**). In the ^{31}P NMR the **a** isomer also always appears at the higher field. In the IR spectra the ν(CO) stretching frequencies of the **a** isomer (CO *trans* to sulfur) of **1**−**4** are consistently lower than those of isomer **b** (CO *trans* to nitrogen), which may be related to the π-donor ability of the sulfur atom. When the complexes **1** and **2** are compared with **3** and **4**, the ν(CO) stretching frequencies are slightly lower in the pyridine-2-thiolate complexes. Complexes **1** and **2** are therefore expected to have more reducing metal centers with more back-bonding into the π*-orbital of the CO ligand.

Ligand Additivity and Electrochemistry. Complexes **1**−**4** were targeted as potential precursors for stable and acidic dihydrogen complexes on the basis of their theoretical electrochemical potentials calculated from Lever's ligand additivity model.[17] In our previous work we showed that one can use the model to make semiquantitative predictions about the stability and acidity of dihydrogen complexes $M(H_2)(L)_5$, where the metal M has a d^6 electron configuration.[18] The dihydrogen complex is expected to be acidic and yet stable against loss of H_2 gas if the redox potential of the corresponding dinitrogen complex is close to 2.0 V vs NHE. The model can be used even if the dinitrogen complex is hypothetical as is the case for $[M(N_2)(CO)(L)(PPh_3)_2]^+$ (M = Ru, Os; L = pyS^-, quS^-). No ligand electrochemical parameters for pyridine-2-thiol or quinoline-8-thiol have been determined to date. These ligand parameters were therefore treated as a linear combination of pyridine (E_L = 0.25 V) or quinoline (E_L = 0.29) and thiophenolate (E_L = −0.53 V), resulting in an approximate value of E_L = −0.28 or −0.24 V, respectively, for the whole chelate. With these parameters the calculated theoretical potentials of the hypothetical dinitrogen complexes are 2.07 V (L = pyS^-) vs NHE and 2.11 V (L = quS^-) for the ruthenium complexes and 1.78 V (L = pyS^-) and 1.83 V (L = quS^-) for the osmium complexes. The ruthenium complexes might be expected to be less stable than the osmium ones because of their more positive potentials.

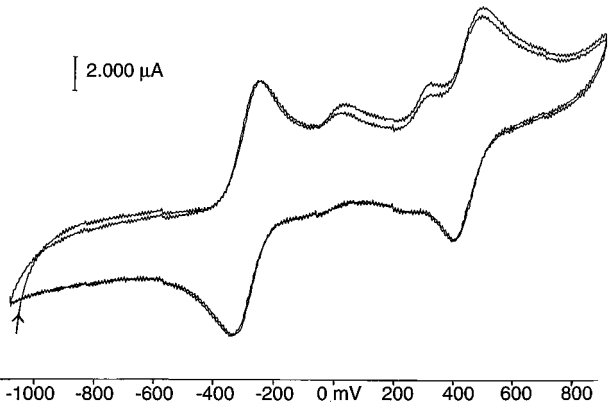

Figure 2. Cyclic voltammogram of **4** in 0.2 M NBu_4PF_6 vs Fc^+/Fc internal standard at 50 mV/s scan rate.

In an attempt to determine the actual ligand parameters for the chelates pyridine-2-thiol and quinoline-8-thiol, the redox potentials of the monohydride complexes **1**−**4** were measured in 0.2 M NBu_4PF_6 in CH_2Cl_2. The complexes display a complex redox chemistry with up to four reversible or irreversible redox processes occurring in the range from −0.6 to +1.6 V vs NHE. Figure 2 shows the cyclic voltammogram of **4** as an example. The measured redox potentials for all four complexes as well as the free thiol ligands are summarized in Table 3. Also listed are the theoretical potentials for **1**−**4** as calculated from the ligand additivity model. In cases where the peaks appear to be reversible or quasi-reversible at 50 mV/s scan rate, the $\Delta E_{1/2}$ values are reported; in all other cases the redox processes are irreversible.[19] It is difficult to determine which of the observed redox processes are metal-based and which are ligand-based. The interpretation of the cyclic voltammograms is further complicated by the presence of the two isomers that may have different redox potentials. It is not clear whether the cyclic voltammograms of the major isomers cover over the peaks of the minor isomers, rendering them undetectable, or whether different peaks for both isomers are present.

The observed cyclic voltammograms clearly demonstrate the limitations of the ligand additivity model. It is only valid for perfectly reversible systems where the HOMO of the complex is completely metal-based, i.e. a filled, nonbonding d orbital.[17] The latter is not necessarily the case for complexes **1**−**4** (*vide infra*). Furthermore, the model does not contain any information about stereochemical relationships in a given ligand set and their influence on the redox potential of the complex. The determination of ligand parameters from the electrochemical data of complexes **1**−**4** is thus not possible.

Reaction of 1−4 with HBF_4·Et_2O at 193 K. Protonation of the monohydride complexes **1**−**4** at low temperature in CD_2Cl_2 can lead to two tautomeric products: protonation of the hydride ligand gives the

(17) Lever, A. B. P. *Inorg. Chem.* **1990**, *29*, 1271−1285.
(18) Morris, R. H. *Inorg. Chem.* **1992**, *31*, 1471−1478.

(19) For the reversible peaks $\Delta E_{1/2}$ is slightly larger than the 59 mV expected for a one-electron process. A calibration run with the internal standard Fc^+/Fc showed this to be an artifact of the cell design and the high uncompensated resistance of the solvent CH_2Cl_2.

Table 3. Observed and Theoretical Redox Potentials *E* for Complexes 1−4 and Free Pyridine-2-thiol and Quinoline-8-thiol[a−c]

	E(obs)	*E*(obs)	E_{pa}(obs)	*E*(obs)	*E*(theor)[d]
Ru(pyS) (**1**)		862 ($\Delta E = 69$)	1173	1420 (E_{pa})	1030
Os(pyS) (**2**)	−31 (E_{pc})	831 ($\Delta E = 220$)	1194		700
Ru(quS) (**3**)	464 ($\Delta E = 69$)	668 ($\Delta E = 69$)	1127		1066
Os(quS) (**4**)	372 ($\Delta E = 86$)	689 (E_{pa})	985	1111 ($\Delta E = 91$)	741
pySH	−263 (E_{pc})		1280		
quSH	−106 (E_{pc})		1300		

[a] All values in mV, referenced against internal standard Fc^+/Fc, reported vs NHE by adding 0.665 V. [b] Conditions: 0.2 M NBu_4PF_6 in CH_2Cl_2, scan rate 50 mV s^{-1}. [c] For reversible/quasi-reversible peaks $E_{1/2}$ and ΔE are listed; otherwise, anodic (E_{pa}) or cathodic (E_{pc}) peak potentials are listed. [d] Calculated using Lever's ligand additivity model with estimated ligand parameters for pyridine-2-thiolate and quinoline-8-thiolate.

dihydrogen complexes $[M(\eta^2\text{-}H_2)(CO)(L)(PPh_3)_2]BF_4$ (**a,b**), while protonation of the sulfur atom leads to the coordinated thiol complexes $[MH(CO)(LH)(PPh_3)_2]BF_4$ (**c**,**d**) (eq 3).

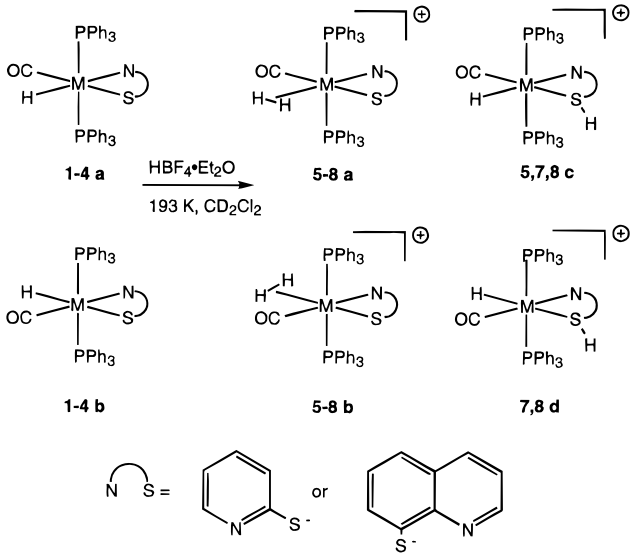

(3)

The addition of acid results in an immediate color change of the CD_2Cl_2 solution from bright yellow to almost colorless for the pyridine-2-thiolate complexes or from deep red to light yellow or orange for the quinoline-8-thiolate complexes. The overall isomer ratios of the protonated complexes {[**a**] + [**c**]}/{[**b**] + [**d**]} always reflect those of the parent monohydride complexes; i.e. there is no acid-mediated flipping of the N,S-chelate between the isomers with CO *trans* to sulfur and CO *trans* to nitrogen.

All the protonated complexes are air- and water-sensitive and, with the exception of **6a,b**, thermally unstable to loss of dihydrogen gas and decomposition. The major isomer **6a** can be isolated by fractional crystallization, and its single-crystal X-ray structure has been obtained.[11] The minor isomer **6b** is stable in solution but loses dihydrogen when precipitated as a solid. This observation mirrors a general qualitative trend observed for the thermally unstable dihydrogen complexes **5**, **7**, and **8**. The isomers **a** (H *trans* to N) form slightly more stable dihydrogen complexes and remain detectable for longer periods of time in the NMR spectrum than the isomers **b**.

At room temperature the ruthenium dihydrogen complexes $[Ru(\eta^2\text{-}H_2)(CO)(L)(PPh_3)_2]BF_4$ (L = pyS^-, **5a,b**; L = quS^-, **7a,b**) instantaneously lose the dihydrogen ligand, leading to rapid and complete decomposition of the sample. The complexes **5a**−**c** and **7a** slowly decompose even at 193 K. **7b**−**d** can be observed up to 273 K. The thiol hydride complex **5d** was not observed. The dihydrogen signal intensity of **5a,b** and **7a,b** decreases with increasing temperature and barely remains above the detection limit in the ^1H NMR at temperatures above 233 K. The osmium complexes **8a**−**d** slowly decompose above 273 K but are stable in solution for hours at lower temperatures. The structural assignments in eq 3 are based on the single-crystal X-ray structure determination of **6a**[11] and the characteristic NMR signals of the dihydrogen and coordinated thiol complexes.

NMR Spectroscopy. A summary of the NMR spectroscopic properties of the complexes **5**−**8** is given in Table 4. With the exception of complexes **6** the spectral appearance at 193 K immediately after addition of excess $HBF_4{\cdot}Et_2O$ is described. At this temperature, inversion of the thiol proton in the coordinated thiol species is arrested or is slow on the NMR time scale. This makes the two phosphorus nuclei, P^x and P^y, inequivalent as illustrated in Figure 3 and results in the observed AXY doublet of doublets pattern of the thiol proton in the organic region of the ^1H NMR as well as the doublets in the $^{31}P\{^1H\}$ NMR spectra. The signals in the ^1H NMR coalesce at 213 K and resharpen above 233 K as 1:2:1 triplets and singlets, respectively. The signal of the thiol proton of **5c** could not be unambiguously identified, but the presence of a thiol hydride complex was inferred by analogy to the quinoline-8-thiol complexes (cf. Table 4) and from the hydride resonance at −13.41 ppm and the ^{31}P NMR pattern. The hydride ligands of the coordinated thiol tautomers appear as binomial triplets below −8 ppm. The dihydrogen ligands give rise to the typically broad resonances observed between −3 and −8 ppm.

The T_1 value for the signal of **5a** at −6.05 ppm at 193 K is 11.4 ± 0.6 ms, establishing **5a** as a dihydrogen complex. The corresponding signals of **5b** and **7a,b** (Table 4) at 198 K are too small to allow a reproducible determination of their T_1 times but are assigned to dihydrogen ligands by analogy to the properties of complexes **6** and **8**. The T_1 minima of the dihydrogen tautomers of the more stable osmium complexes **6a** and **8a** have been reported previously.[3,11] They are 16 ± 1 ms at 241 K and 14.3 ± 0.2 ms at 233 K (both values at 400 MHz). The T_1 time (400 MHz) of **8b** has only been determined at 273 K. At this temperature it is 17.8 ± 0.6 ms. Attempts to synthesize the η^2-HD isotopomers of complexes **5a,b**, **7a,b**, and **8a,b** by reaction with either $DBF_4{\cdot}Et_2O$ or a $HBF_4{\cdot}Et_2O/D_2O$ mixture at low

Table 4. ^{1}H and ^{31}P NMR Spectroscopic Data of Complexes 5−8 (δ in ppm, J in Hz)

		^{1}H NMR		
	yield (%)	hydride/ η^2-H_2	thiol proton	^{31}P NMR[c]
5a[a]	∼75	−6.05 (br)		36.24 (s)
5b[a]	∼10	−7.30 (br)		40.24 (s)
5c[a]	∼15	−13.41 (t, $^2J_{HP}$ = 18.6)	*d*	40.79 (br), 49.63 (br)
6a[b]	65	−5.70 (br)		9.07 (s)
6b[b]	35	−6.84 (br)		11.77 (s)
7a[a]	∼2	−7.5 (br)		33.34 (s)
7b[a]	∼10	−5.40 (br)		27.20 (s)
7c[a]	∼23	−11.51 (t, $^2J_{HP}$ = 15.4)	4.35 (dd, $^2J_{HP^x}$ = 19.4, $^2J_{HP^y}$ = 6.7)[e]	55.19 (d, $^2J_{PP}$ = 247.5), 46.76 (d, $^2J_{PP}$ = 246.3)[e]
7d[a]	∼65	−8.11 (t, $^2J_{HP}$ = 17.8)	4.51 (dd, $^2J_{HP^x}$ = 21.8, $^2J_{HP^y}$ = 8.5)[e]	55.59 (d, $^2J_{PP}$ = 248.2), 48.09 (d, $^2J_{PP}$ = 248)[e]
8a[a]	∼25	−6.3 (br)		8.23 (s)
8b[a]	∼15	−3.30 (br)		0.93 (s)
8c[a]	∼10	−13.04 (t, $^2J_{HP}$ = 15.9)	4.95 (dd, $^2J_{HP^x}$ = 21.4, $^2J_{HP^y}$ = 14.2)[e]	not resolved (overlap with **8d**)
8d[a]	∼50	−9.34 (t, $^2J_{HP}$ = 17.6)	5.17 (dd, $^2J_{HP^x}$ = 13.2, $^2J_{HP^y}$ = 6.8)[e]	29.12 (d, $^2J_{PP}$ = 233.7), 21.54 (d, $^2J_{PP}$ = 233.8)

[a] Conditions: CD_2Cl_2, 300 or 400 MHz, 193 K, excess HBF_4. [b] $CDCl_3$, 400 MHz, 298 K. [c] $CD_2Cl_2/CDCl_3$, 300 MHz (121 MHz for ^{31}P), relative to 85% H_3PO_4. [d] Signal obscured by pyridine-2-thiolate/thiol resonances. [e] Cf. Figures 3 and 4.

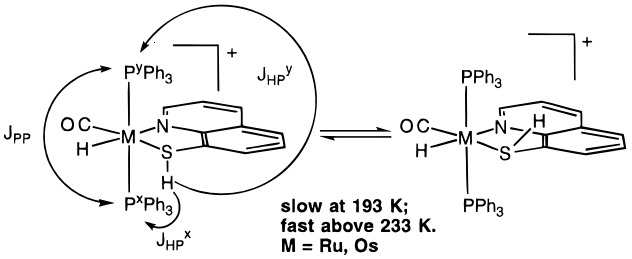

Figure 3. Orientation of the thiol proton in complexes **c**,**d** and resulting NMR coupling pattern (only one isomer shown).

temperature were unsuccessful. Only for the stable complex **6a** could a J(HD) coupling value of 21 Hz be observed.[11] When the protonation reactions were carried out under an atmosphere of D_2 in the presence of excess HBF_4, no isotope exchange to form the HD complexes was observed.

Heteronuclear Decoupling Experiment. The spectral assignments of the thiol hydride complexes made in Table 4 were confirmed by a heteronuclear decoupling experiment performed on **7c**,**d** at 193 K and 300 MHz. This was done by observing the effects of selective irradiation of ^{31}P signals on the ^{1}H NMR signals of the thiol proton in the organic region and the hydride in the high-field region in the spectrum of **7c**,**d**. Figure 4 shows the ^{31}P NMR spectrum of **7c**,**d** at 193 K and its schematic representation. The spectrum consists of two sets of doublets with J_{PP} = 247 Hz (**7d**) (peaks 1−4) for the major isomer and a similar set with J_{PP} = 248 Hz (**7c**) (peaks 5−8) for the minor isomer. The singlet at 44.65 ppm is probably the transient five-coordinate complex [Ru(CO)(quS)(PPh_3)$_2$]BF_4, generated from loss of H_2 gas from **7a,b**, whose signals appear further upfield. As shown in Figure 5, the irradiation of peak 3 or 4 causes the hydride triplet at −8.81 ppm and the doublet of doublets pattern of the thiol proton at 4.51 ppm in the ^{1}H NMR to collapse to doublets, leaving all other peaks unaffected. This proves the correlation of the affected signals which are assigned to the coordinated thiol complex **7d**. The irradiation of peak 1 or 2 causes all triplets and doublets of doublets to collapse into doublets. In this case the bandwidth of the decoupler is too wide to discriminate between the minor and major isomer. Complexes **8c**,**d** show the same resonance patterns in the ^{1}H and ^{31}P NMR, and the spectral assignments in Table 4 are made by analogy.

Tautomeric Equilibria and Tautomer Ratios. In

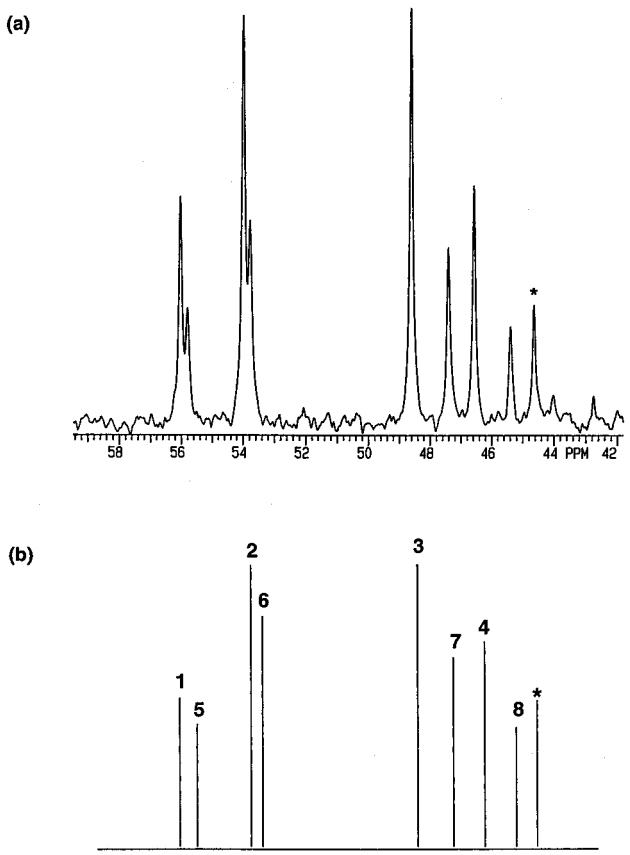

Figure 4. (a) ^{31}P{^{1}H} NMR spectrum of **7c**,**d** at 193 K. (b) Schematic representation of the spectrum. peaks 1−4, **7d**; peaks 5−8, **7c**.

all cases except for **2**, which selectively gives the dihydrogen complexes [Os(η^2-H_2)(CO)(pyS)(PPh_3)$_2$]BF_4 (**6**), mixtures of the two possible tautomers are formed as in eq 3. The hypothetical thiol hydride complexes **6c**,**d** are also not observed at low temperature. Column 2 of Table 4 lists typical percentages of the tautomers observed at 193 K in the presence of excess acid. The major tautomer at 193 K in the pair **5a,c** is the dihydrogen form. The reaction mixture of complexes **7** at this temperature is almost entirely dominated by the thiol hydride tautomers. Only minimal amounts of the dihydrogen tautomers are formed, in concentrations close to the detection limit in the ^{1}H NMR spectrum. The ruthenium complexes **5** slowly decompose even at 193 K, which also influences the observed tautomer distribution. Any changes in the appearance of the

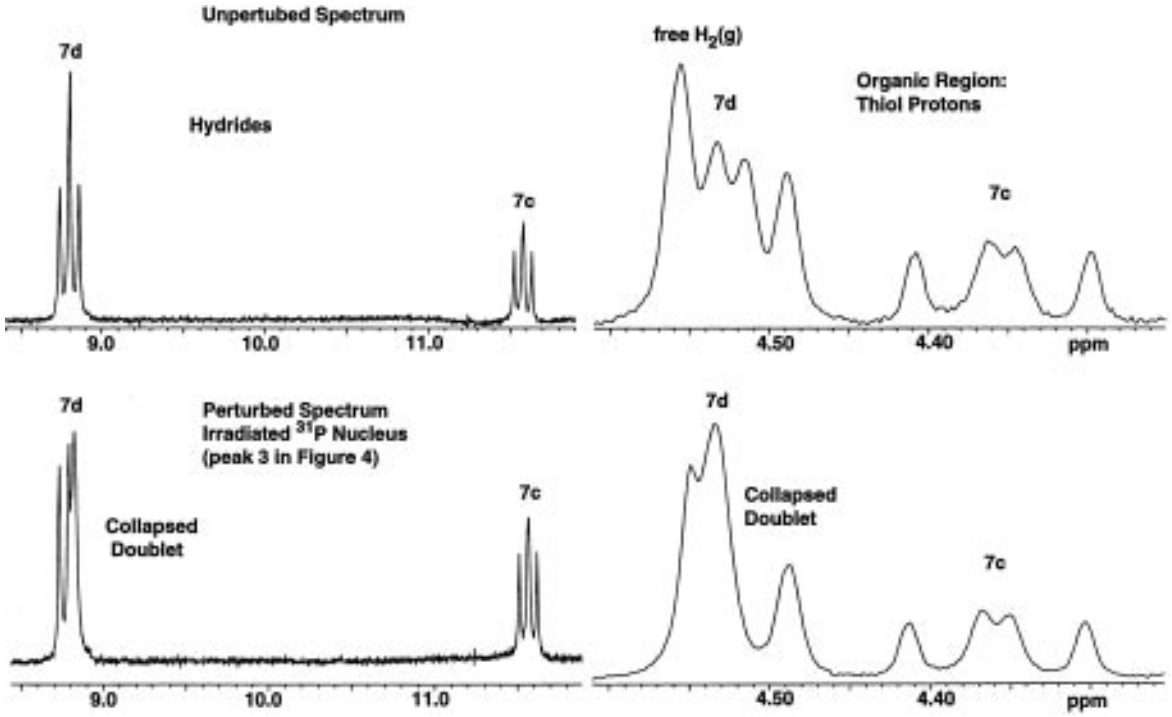

Figure 5. ^{1}H NMR organic and hydride regions of **7c**,**d** at 193 K, showing the effect of selective decoupling of the ^{31}P peak 3 in Figure 4.

Table 5. Tautomer Distributions of 8a−d at 193 K in CD_2Cl_2 as a Function of Acid Concentration[a]

	[HBF_4]	[**a**] + [**c**]	[**b**] + [**d**]	[**a** + **b** + **c** + **d**]/[HBF_4]	[**a**]/[**c**]	[**b**]/[**d**]
~2-fold excess acid	4.31	1.00	3.50	1.04	2.51	0.17
~0.1-fold excess acid	0.61	1.00	3.64	7.58	2.49×10^{-3}	0.12

[a] Determined from the ^{1}H NMR integration of acid and hydride signals (normalized to the total concentration [**a**] + [**c**] of the minor isomer **8a,c**).

spectra of the protonated ruthenium complexes **5** and **7** with increasing temperature are completely irreversible and are driven by decomposition processes which mask the evolution of a possible tautomeric equilibrium with temperature. Therefore, no quantitative interpretation of the tautomer distributions as a function of temperature in the ruthenium complexes **5** and **7** was attempted.

The observation of the tautomeric equilibrium in eq 4[3] is limited to the thermally more stable osmium complexes **8a**−**d**.

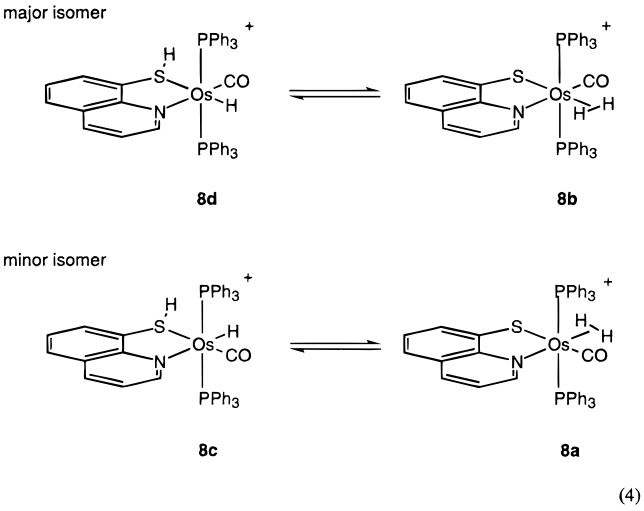

(4)

In a series of experiments with these complexes we found that the observed tautomer ratios in the reaction mixtures depend not only on temperature but also heavily on the acid concentration. The reproducibility of individual reactions under the same conditions is limited. Control of the effective acid concentration in the sample proved to be extremely difficult, even if nominally equimolar amounts of $HBF_4 \cdot Et_2O$ solution were added using a microliter syringe. Small changes in temperature that occur during the transfer of the cold sample into the probe of the NMR spectrometer at low temperature also appear to influence the tautomer distribution. Furthermore, at 193 K the viscosity of the CD_2Cl_2 solution may influence the effective rate of the reaction of **4** with acid, if the protonation occurs under kinetic control. The last two effects are beyond experimental control.

Only in one experiment was an approximately equimolar amount of acid achieved (*vide infra*). In all other experiments an excess amount of acid was present. If a less than equimolar amount of HBF_4 is present, the resonances in the hydride region coalesce completely, but if excess acid is subsequently added, they resharpen to the set of resonances listed in Table 4. Two sets of observed tautomer distributions at 193 K are listed in Table 5: one with a ~2 fold excess of HBF_4 relative to the total amount of monohydride complexes, and the other with an essentially equimolar amount (~0.1-fold excess). The relative concentrations were determined from the integral values of the hydride and dihydrogen resonances and are reported relative to the total concentration of the minor isomer tautomers **8a,c**; i.e., the concentration [**8a**] + [**8c**] equals unity. The tempera-

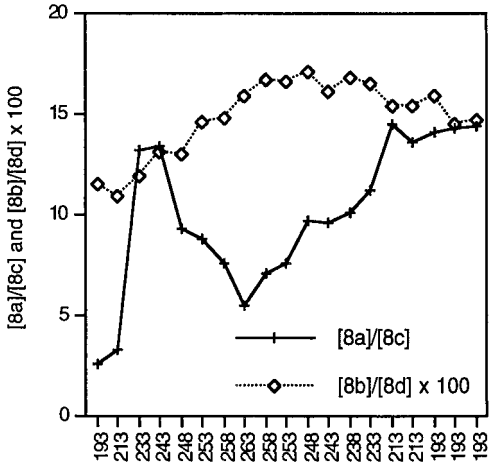

Figure 6. Plot of [**8a**]/[**8c**] and [**8b**]/[**8d**] as a function of temperature in the presence of a ~1.5-fold excess of HBF_4.

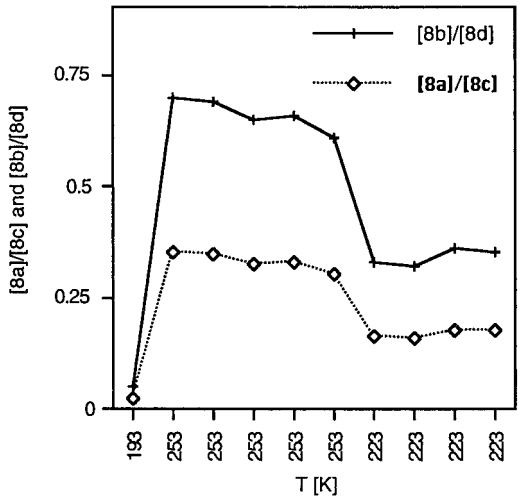

Figure 7. Plot of [**8a**]/[**8c**] and [**8b**]/[**8d**] as a function of temperature in the presence of a ~0.1-fold excess of HBF_4.

ture responses of the tautomeric equilibria between **a** and **c** as well as **b** and **d** also depend on the free acid concentration. Figures 6 and 7 show plots of the concentration ratios [**8a**]/[**8c**] and [**8b**]/[**8d**] as the temperature is stepped up and then down in 10 min intervals for experiments with ~2- and ~0.1-fold excesses of acid, respectively. The 10 min waiting period between data points allows for complete equilibration of the system. Estimated errors are less 5% of absolute values and error bars are omitted for clarity. The data in Figure 6 for the minor isomer are the same as in Figure 2 of ref 3. The numeric values of the tautomer ratio [**8b**]/[**8d**] of the major isomer are multiplied by a factor of 100. Thus, both tautomer ratios can be plotted approximately on the same scale. Figure 7 also illustrates the thermal lability of the system even at 253 K. The slight decrease of the tautomer ratios over the course of approximately 40 min at this temperature is due to slow degradation of the sample.

Independent of the acid concentration, the tautomer ratio [**8b**]/[**8d**] of the major isomer is smaller than 1. There is always more of the thiol hydride than of the dihydrogen tautomer present, and the ratio increases with higher temperature. In the presence of excess acid the temperature response is, however, only weakly expressed and is not completely reversible (Figure 6).

In contrast, the observed tautomer ratio of the minor isomer [**8a**]/[**8c**] shows a strong dependence on temperature changes in both cases and the temperature response of the equilibrium inverts, depending on the acid concentration. In the presence of an ~2-fold excess of acid relative to the total amount of monohydride complexes, there is more of the dihydrogen tautomer formed at 193 K. There is a large increase of the ratio [**8a**]/[**8c**] when the reaction mixture is warmed from 213 to 233 K. This suggests that in the presence of excess acid the initial tautomer distribution at low temperature is produced under kinetic control. Under equilibrium conditions above 233 K the tautomer ratio favors the thiol hydride complex with increasing temperature. The opposite temperature response is observed if an approximately equimolar amount of HBF_4 is added. In this case very little dihydrogen tautomer is initially formed at 193 K, but it is clearly favored at higher temperatures. In both cases the temperature response of the minor isomer tautomers is strong and shows good reversibility. The relatively poor data quality on the temperature response of the equilibria allows only a qualitative interpretation of the resulting van't Hoff plots. In the presence of excess or equimolar amounts of acid ΔH for K = [**8a**]/[**8c**] falls between 100 and 200 or −130 and −260 kJ/mol, respectively. ΔS is smaller than 1 J K^{-1} mol^{-1} in both cases; i.e., the equilibrium is essentially enthalpy-driven. The ΔH and ΔS values for K = [**8b**]/[**8d**] were only determined from the data in Figure 7 (equimolar amount of acid) and are identical with the those of the pair **8a,c** in the same experiment.

A spin saturation transfer experiment on the isomer and tautomer mixture of **8** in the presence of an ~2-fold amount of acid was carried out at 263 K. Selective decoupling of the dihydrogen signals of **8a,b** or the well-resolved thiol hydride triplets of **8c**,**d** had no effect on the spectral appearance, whereas irradiation of the signal of free HBF_4 at 11 ppm resulted in a reduction of the thiol proton signals of **8c** at 4.83 ppm and **8d** at 5.16 ppm by 100% and 36%, respectively. (At 263 K the signals are shifted 0.25 ppm upfield from the values at 193 K in Table 4.) In the difference spectrum (perturbed minus unperturbed system) these signals are integrated to approximately the same value. This establishes that in the presence of excess HBF_4 proton exchange occurs intermolecularly between free excess acid and the coordinated thiol form and is faster for the minor isomer. Intramolecular or intermolecular proton exchange involving the dihydrogen tautomers is not observed in the presence of excess acid and is therefore slow on the NMR time scale; i.e., the rate constant k_{ex} of such a process is at least 5 times smaller than the relaxation rate $1/T_1$ of the dihydrogen ligand. This is consistent with the observed short T_1 of the dihydrogen ligands of **8a** and **8b**,[3] which otherwise would be averaged with the much longer T_1 of either the thiol proton of the coordinated thiol tautomer or the free acid. In the one experiment in which an approximately equimolar amount of acid was present, the hydride signals of the thiol hydride tautomers **8c**,**d** are broadened above 233 K and not resolved into triplets. In this case the proton exchange possibly occurs intramolecularly.

Acidity of [Os(η^2-H_2)(CO)(pyS)(PPh_3)$_2$]BF_4 (6a). We previously reported that in $CDCl_3$ solution complex **6a** is deprotonated by water but not by Et_2O. The pK_a

of **6a** is therefore estimated to be about −2 on an aqueous scale, falling between the extreme values of −2.4 (pK_a of Et_2OH^+)[20] and −1.74 (formal pK_a of H_3O^+).[21] A calorimetric titration study of the reaction of the isomeric mixture **2** with CF_3SO_3H in 1,2-dichloroethane (1,2-DCE) was carried out by Wang and Angelici (eq 5).

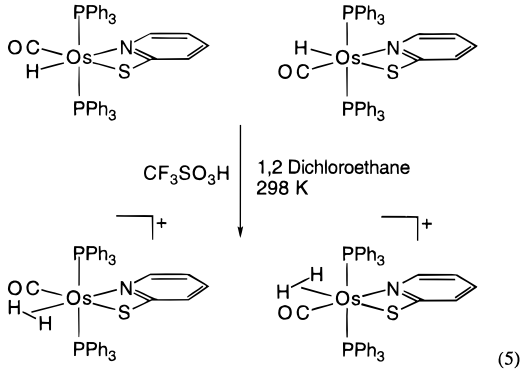

(5)

The enthalpy of protonation ΔH_{HM} of **2** under standard conditions (298 K) is −15.9 kcal/mol.[22] Using the linear relationships between pK_a and ΔH_{HM} values established for amine and phosphine bases by Angelici and co-workers,[23] the possible pK_a range of **6** can be defined. The assumption that **2** behaves like an N-base leads to a pK_a of −3.1, while assuming it behaves as a P-base leads to pK_a value of −0.2. The complex is protonated at neither a nitrogen nor a phosphorus atom but, instead, at the metal or hydride ligand. We note, however, that the independently measured pK_a of approximately −2 falls in the middle of the range derived from the calorimetric study.

Relative Acidities of the Complexes. The reaction of **6a** with the parent monohydrides **1** and **4** allows a qualitative comparison of the relative acidities of the osmium vs ruthenium and pyridine-2-thiol vs quinoline-8-thiol complexes, respectively. Combining solutions of the two complexes with a solution of **6a** leads to an instantaneous decolorization of purple monohydride **4** to a light yellow or lightening of the yellow color of **1** to almost colorless, indicating complete protonation of **4** or **1** to give the series of complexes **5** or **8**.

The reaction of a slight excess of **6a** with **1** in CH_2Cl_2 was carried out at 213 K and followed by ^{31}P NMR (300 MHz). The reaction mixture at low temperature immediately after mixing is composed of **2a**, **5a,b**, and **6a** (eq 6).

The NMR signals of **2a** and **5a,b** are broadened and shifted toward each other by ∼1 ppm, indicating proton exchange between the two species, while the signal of the excess, unreacted **6a** remains sharp. No **5c** or **5d** is observed; thus, the products reflect the relative acidities of the dihydrogen complexes. At higher temperatures the reaction is no longer an acid/base equilibrium but is driven by decomposition of the **5a,b** formed in the reaction. The peak of the excess **6a** persists at room temperature. Approaching the acid/base equilibrium from the other side, i.e. reacting **5a,b** with **2**, is not feasible since the ruthenium dihydrogen complexes cannot be isolated. On the basis of IR ν(CO) stretching frequencies of the parent monohydride complexes **1a,b** and their more positive theoretical redox potentials, the ruthenium complexes would have been expected to form the more acidic dihydrogen complexes. The higher acidity of the osmium complex **6** vs the ruthenium complex **5** may therefore be a consequence of stronger H−H bonding in the dihydrogen ligand of the ruthenium complex.[24]

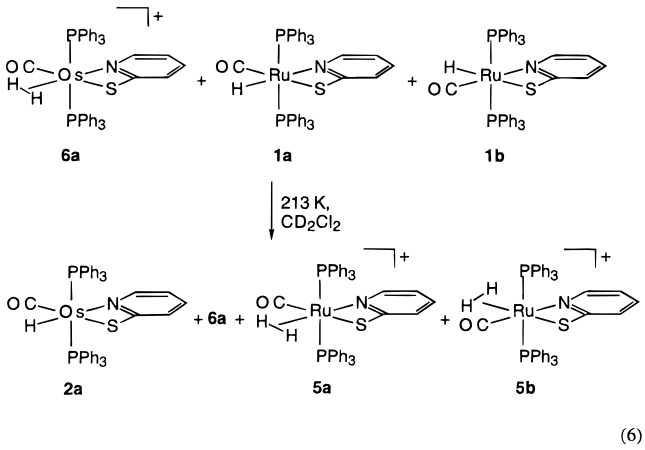

(6)

In order to study the effect of the ligands pyridine-2-thiolate vs quinoline-8-thiolate on the acidity of the complexes, the complex **6a** was reacted with the isomeric mixture of complex **4** (eq 7).

$$\mathbf{6a} + \mathbf{4a} + \mathbf{4b} \xrightarrow[298\ K]{CD_2Cl_2} \mathbf{2a} + \mathbf{8a} + \mathbf{8b} + \mathbf{8c} + \mathbf{8d} \quad (7)$$

Because of the higher stability of the protonated osmium complexes the reaction can be carried out at room temperature, if the NMR spectrum is recorded immediately after mixing, before significant decomposition occurs. The ^{31}P NMR at 293 K shows a single, very broad resonance from 17.4 to 30.4 ppm. The broad resonance suggests fast proton exchange between **2a** and the coordinated thiol complexes **8c**,**d**, whose ^{31}P NMR signals appear in this region. Two sharp singlets at 2.1 and 3.4 ppm are assigned to **8b** and **8a,** respectively. Their signals are shifted from the values observed at 193 K (cf. Table 4), and their assignments were confirmed independently from a sample of protonated **4** at room temperature. In comparison to the coordinated thiol tautomers their signals are well-resolved and proton exchange with these complexes appears to be slow on the NMR time scale. This is also consistent with the findings from the tautomeric equilibria experiments.

In summary, **6a** is more acidic than the corresponding ruthenium dihydrogen complexes **5a,b** and the series of dihydrogen and thiol hydride complexes **8a**−**d**. The complementary reactions of **7** with **4** or **8** with **3** are not feasible, since none of the protonated species can be isolated.

X-ray Crystal Structure Determination and NMR Properties of $[Os(CO)(\mu_2\text{-Spy})(SpyH)(PPh_3)]_2[BF_4]_2$ (9). X-ray grade crystals of the dimeric complex **9** were

(20) Perdoncin, G.; Scorrano, G. *J. Am. Chem. Soc.* **1977**, *99*, 6983−6986.

(21) Lowry, T. H.; Richardson, K. S. *Mechanism and Theory in Organic Chemistry*; Harper & Row: New York, 1987.

(22) Wang, D.; Angelici, R. J. Personal communication, 1994.

(23) Sowa, J. R. J.; Bonanno, J. B.; Zanotti, V.; Angelici, R. J. *Inorg. Chem.* **1992**, *31*, 1370−1375.

(24) Cappellani, E. P.; Drouin, S. D.; Jia, G.; Maltby, P. A.; Morris, R. H.; Schweitzer, C. T. *J. Am. Chem. Soc.* **1994**, *116*, 3375−3388.

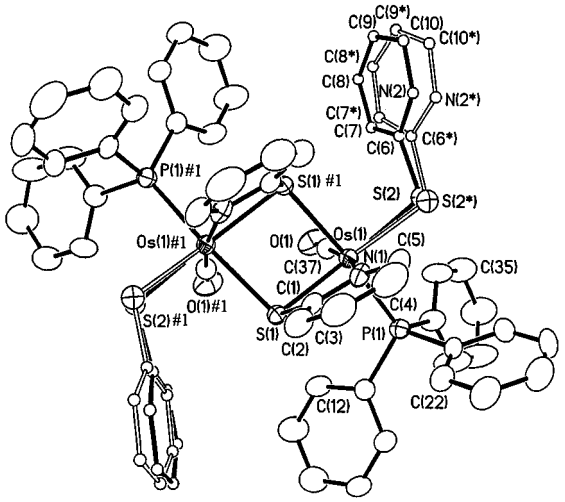

Figure 8. View of the structure of the cation of **9** at the 50% probability level.

Table 6. Selected Bond Lengths (Å) and Angles (deg) in $[Os(CO)(\mu_2\text{-Spy})(SpyH)(PPh_3)]_2[BF_4]_2$ (9)

Os(1)−P(1)	2.3093(14)	Os(1)−N(1)	2.120(4)
Os(1)−C(37)	1.885(5)	C(37)−O(1)	1.128(6)
Os(1)−S(1)	2.4303(13)	Os(1)−S(1)#1	2.4813(13)
Os(1)−S(2)	2.369(3)	Os(1)−S(2*)	2.432(4)
C(1)−S(1)	1.768(5)	C(1)−N(1)	1.372(7)
C(6)−S(2)	1.732(10)	C(6*)−S(2*)	1.716(13)

S(1)−Os(1)−S(1)#1	80.25(4)	Os(1)−S(1)−Os(1)#1	96.23(4)
S(2)−Os(1)−S(1)	159.38(11)	S(2*)−Os(1)−S(1)	151.1(2)
S(2)−Os(1)−S(1)#1	93.49(8)	S(2*)−Os(1)−S(1)#1	95.36(10)
S(1)−Os(1)−N(1)	67.42(13)	S(1)#1−Os(1)−N(1)	88.87(12)
S(2)−Os(1)−N(1)	93.0(2)	S(2*)−Os(1)−N(1)	84.0(2)
N(1)−Os(1)−C(37)	169.3(2)	S(1)−Os(1)−C(37)	102.4(2)
S(1)−Os(1)−P(1)	95.64(5)	S(1)#1−Os(1)−P(1)	173.77(5)
S(2)−Os(1)−P(1)	91.96(8)	S(2*)−Os(1)−P(1)	90.49(10)
Os(1)−S(1)−C(1)	81.3(2)	Os(1)#1−S(1)−C(1)	109.4(2)
Os(1)−S(2)−C(6)	109.9(4)	Os(1)−S(2*)−C(6*)	110.3(5)

obtained from **6a,b** in CH_2Cl_2/Et_2O in the presence of excess HBF_4 and on exposure to air. **9** crystallizes in the monoclinic space group *C*2/*c* with $a = 28.287(3)$ Å, $b = 10.1513(14)$ Å, $c = 25.185(3)$ Å, $\beta = 116.578(8)°$, $V = 6467.6(14)$ Å^3, and $Z = 4$. Since **9** contains two pyridine-2-thiol ligands but only one PPh_3 ligand per osmium center, it is a nonstoichiometric decomposition product of the dihydrogen complexes **6a,b**. The structure of **9** is shown in Figure 8. Two rotationally disordered BF_4^- counterions and two CH_2Cl_2 solvent molecules are omitted for clarity. In the chosen orientation the C_2 symmetry axis running through the center of the dimer is perpendicular to the plane of the page. Selected bond lengths and angles are listed in Table 6. The core of the dimer consists of a four-membered ring containing the two osmium atoms of the monomeric units with the sulfur atoms of the chelating pyridine-2-thiolates as the bridging atoms. The osmium sulfur distances Os(1)−S(1) and Os(1)−S(1)#1 in the ring are nonequivalent. They are 2.430(1) and 2.481(1) Å, respectively. By comparison, the osmium−sulfur distance of the nonbridging chelating pyridine-2-thiolate ligand in the structure of **6a** is 2.450(3) Å.[11] The ring defined by the osmium and sulfur atoms is not planar with a mean deviation of 0.2143 Å from an idealized plane. The bond angles Os(1)−S(1)−Os(1)#1 and Os(1)−S(1)−C(1) are 96.23(4) and 81.3(2)°. The osmium−nitrogen distance is 2.120(4) Å, compared to 2.070(3) Å in **6a**, and the angles N(1)−Os(1)−S(1) and N(1)−Os(1)−S(1)#1 are 67.4(1) and 88.8(1)°. The distorted-octahedral coordination sphere of each of the osmium centers is completed by a CO ligand *trans* to the nitrogen atom of the chelate, a triphenylphosphine ligand, and a monodentate coordinated pyridine-2-thiol ligand. Interestingly, both bridging pyridine-2-thiolate ligands are located on the same side of the molecule. The analogous bridged $M_2(\mu_2\text{-Spy})_2$ core with such parallel pyridine rings has been observed by us in the iridium dimer $[IrH(\mu_2\text{-Spy})(SpyH)(PCy_3)]_2[BF_4]_2$ (SpyH = mercaptopyridinium[25]) and in the similar quinoline-8-thiolate complex $[Re_2H_6(\mu\text{-Squ})_2(PPh_3)_4]^+$ by Leeaphon et al.[26] Such an arrangement is apparently favorable for steric reasons. There is a nonchelating sulfur-coordinated mercaptopyridinium ligand in each monomeric unit, which is disordered over two sites with relative occupancies of 44:56. An isotropic refinement of the disordered ligand gave bond angles Os(1)−S(2)−C(6) and Os(1)−S(2*)−C(6*) equal to 109.9(4) and 110.3(5)° and carbon−sulfur distances C(6)−S(2) and C(6*)−S(2*) of 1.732(10) and 1.716(13) Å, respectively. The apparently more sp^3-like hybridization of the sulfur atom is more consistent with a zwitterionic mercaptopyridinium than with a thione formulation. This has also been suggested for the complexes $CoCl_2(SpyH)_2$[27] and $[Cu(SpyH)_3]NO_3$.[28] Coordination to the metal stabilizes a partial negative charge on the sulfur and thereby allows the ligand to retain a higher degree of aromaticity. This formulation is also in agreement with the observed C-C bond distances in the ring, which vary only between 1.35 and 1.44 Å, compared to 1.29 and 1.52 Å in the free nonaromatic thione.[27] There is residual electron density in the difference map near the nitrogen atom of the mercaptopyridinium ligand, but due to the effects of the disorder in the ligands and the counterion BF_4^-, attempts to refine the position of the proton were unsuccessful. The ^{31}P NMR of **9** shows a single peak at 9.62 ppm for the two equivalent PPh_3 ligands, in agreement with the C_2 symmetry of the dimer. A distinct resonance in the ^1H NMR of the crystal sample appears at 13.00 ppm. This value is close to the 13.48 ppm observed for the N−H proton of free dimeric pyridine-2-thione in $CDCl_3$[12] and therefore probably represents the N−H proton of the mercaptopyridinium ligand.

Discussion

Influence of the Chelate Ligand on the Isomer Distribution of the Monohydride Complexes 1−4. The nature of the chelating thiolate ligand has a decisive influence on the isomer distribution in the monohydride complexes $MH(CO)L(PPh_3)_2$ (**1**−**4**). The isomer ratio in the pyridine-2-thiolate complexes **1** and **2** favors isomer form **a**, in which the hydride ligand is *trans* to the nitrogen atom of the chelate, whereas in the quinoline-8-thiolate complexes **3** and **4**, isomer form **b** dominates, in which the hydride ligand is *trans* to the sulfur atom of the chelate. There is no distinct influence of the metal on the isomer distribution (cf. Table 2).

(25) Park, S.; Ramachandran, R.; Morris, R. H. Unpublished results, 1995.
(26) Leeaphon, M.; Ondracek, A. L.; Thomas, R. J.; Fanwick, P. E.; Walton, R. A. *J. Am. Chem. Soc.* **1995**, *117*, 9715−9724.
(27) Binamira-Soriaga, E.; Lundeen, M.; Seff, K. *Acta Crystallogr., Sect. B* **1979**, *35*, 2875−2879.
(28) Kokkou, S. C.; Fortier, S.; Rentzeperis, P. J.; Karagiannidis, P. *Acta Crystallogr., Sect. C* **1983**, *39*, 178−180.

Mura et al. suggested that the observed isomer distribution in the synthesis of **1** and **2** is thermodynamically controlled.[12] This was based on their observation that identical isomer distributions are obtained if the reaction is carried out with the disulfide pyS−Spy instead of free pyridine-2-thiol. Under the very similar reaction conditions employed in the synthesis of **3** and **4**, the isomer distribution is probably also governed by thermodynamics.

Under thermodynamic control the inversion of the isomer distribution in **3** and **4** relative to **1** and **2** directly reflects the relative stabilities of the respective isomers. Since the complex fragment $MH(CO)(PPh_3)_2$ remains unchanged, this must be an immediate consequence of the nature of the chelating ligand. The enlarged ring size has two effects: the bite angle of the chelate widens and the formal charge distribution in the corresponding thiolate changes. In the pyridine-2-thiolate ligand the charge can formally be located on either of the donor atoms, whereas in quinoline-8-thiolate the formal charge must remain on the sulfur atom to avoid an energetically unfavorable location of charge on a carbon atom of the ring system. Consistent with this is the tendency of the free pyridine-2-thiol to be in tautomeric equilibrium with its thione form in nonpolar solvents, predominantly as a hydrogen bonded dimer of the thione. This is unfavorable for quinoline-8-thiol.

The formal charge distributions in the anionic quinoline-8-thiolate, pyridine-2-thiolate, and its mesomer 2-thioxopyridyl (thioxo denotes S═) qualitatively correlate with the electron density distributions in their HOMO's. Figure 9 shows CACAO[29] generated diagrams of the HOMO of the free anions obtained from EHMO level calculations.[30,31] The largest coefficient of electron density in the HOMO of the quinoline-8-thiolate anion is located in a p_z AO on the sulfur donor atom, while there is little electron density on the nitrogen. The electron distribution in pyridinethiolate reacts sensitively to the carbon−sulfur bond length. The two diagrams represent the two extremes of a continuum between a pure thiolate form with a large coefficient on the sulfur and small coefficient on the nitrogen atom and a pure thione form with coefficients of approximately the same magnitude on both donor atoms. Notable is the change in symmetry of the AO on the sulfur atom. In the thiolate mesomer it has π-symmetry with respect to the aromatic ring and the d orbitals of a metal when coordinated. In the 2-thioxopyridyl mesomer it has σ-symmetry.

Some qualitative insight into the electron distribution in the frontier orbitals of the monohydride complexes as a function of the chelating ligand can be gained from EHMO calculations on the simplified complex $OsH(CO)(pyS)(PH_3)_2$ (**2a***), in which the PPh_3 ligands have been replaced with PH_3 to allow use of the CACAO program. Approximate structural data for this complex are available from the single-crystal X-ray structure of **6a** and were used as a starting point in the calculations. A problematic point is the direct influence of the hydride vs the dihydrogen ligand on the bond length of the *trans*-positioned osmium-nitrogen bond. We recently showed

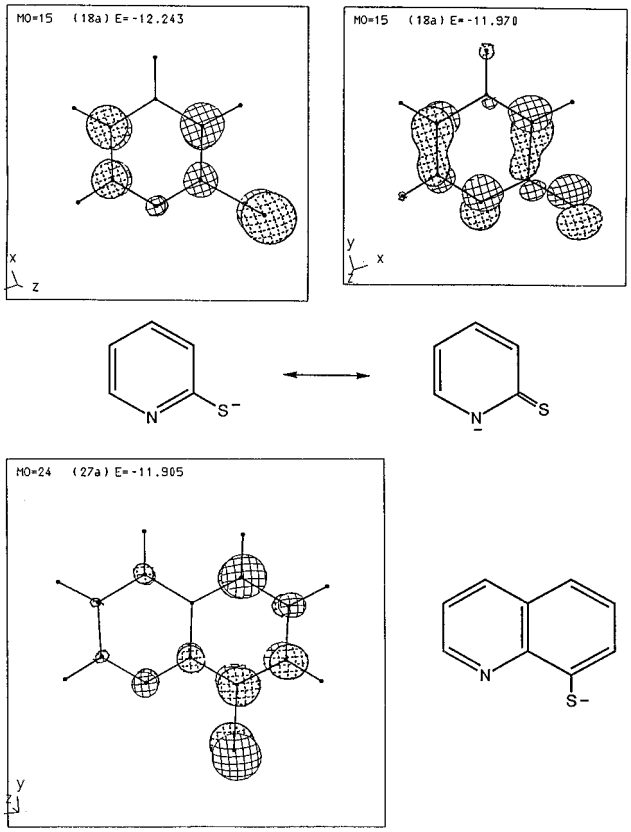

Figure 9. CACAO generated diagrams of the HOMO representing the formal charge distribution in pyridine-2-thiolate and quinoline-8-thiolate.

that the osmium-nitrogen bond in the complex $[OsH(CH_3CN)(dppe)_2]BF_4$ shortens by 0.04 Å upon formation of the corresponding dihydrogen complex $[Os(\eta^2\text{-}H_2)(CH_3CN)(dppe)_2](BF_4)_2$.[32] The structural data from the X-ray structure of **6a** should, however, suffice for a qualitative discussion of the electronic structure of the high-lying filled orbitals of **2** at the EHMO level.

Figure 10 shows CACAO generated diagrams of the HOMO (MO #30) of **2a*** and the two filled MO's closest in energy, #31 and #32 (MO's are numbered in order of decreasing energy; the total number of MO's is 64). The HOMO is primarily composed of a metal d orbital with some electron density in the carbon π-system of the chelate. The filled MO closest in energy to the HOMO (MO #31) has a large coefficient on the sulfur atom and a π-bonding interaction between a d orbital on the metal and the carbonyl ligand. The latter is also present in MO #32. No structural data for complexes **1a,b**, **2b**, **3a,b**, and **4a,b** are available. Sample calculations on these complexes assuming a range of standard bond lengths and angles[33,34] and an idealized octahedral coordination geometry showed that the filled frontier orbitals are narrowly spaced in energy and are similar in shape to those of **2a***. The magnitude of individual coefficients on the donor atoms and the energetic ordering of orbitals are sensitive to metal donor atom bond parameters, such as the chelate bite angle of the quinoline-8-thiolate ligand and the relative position of

(29) Mealli, C.; Prosperio, D. M. *J. Chem. Educ.* **1990**, *67*, 399−402.
(30) Hoffmann, R.; Lipscomb, W. N. *J. Chem. Phys.* **1962**, *36*, 2179−2189, 3489−3493.
(31) Hoffmann, R. *J. Chem. Phys.* **1963**, *39*, 1397−1412.
(32) Schlaf, M.; Maltby, P. A.; Lough, A. J.; Morris, R. H. *Organometallics* **1996**, *15*, 2270−2278.
(33) Allen, F. H.; Kennard, O.; Watson, D. G.; Brammer, L.; Orpen, A. G.; Taylor, R. *J. Chem. Soc., Perkin Trans. 2* **1987**, S1−S19.
(34) Orpen, A. G.; Brammer, L.; Allen, F. H.; Kennard, O.; Watson, D. G.; Taylor, R. *J. Chem. Soc., Dalton Trans.* **1989**, S1−S83.

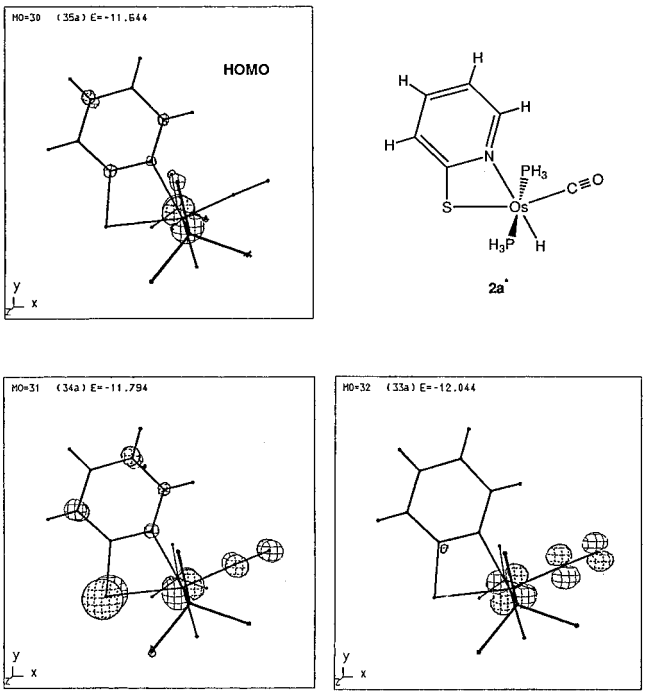

Figure 10. CACAO generated diagram of the HOMO of complexes **2a*** and the two filled orbitals closest in energy.

the carbonyl ligand. However, as a trend we found that the quinoline-8-thiolate complexes are more likely to have a HOMO or other high-lying filled orbitals with substantial coefficients on the sulfur atom than the pyridine-2-thiolate complexes.

The presence of several high-lying metal- and/or sulfur-centered orbitals including the HOMO and their narrow energetic spacing correlates with the observed, complicated, and largely irreversible redox chemistry of **1**−**4**. Removal of electrons from ligand-based orbitals could open reaction pathways that lead to degradation of the ligand framework and decomposition of the complex. A simple reversible redox behavior would be expected if the HOMO is of pure metal d character.

Relative Stability and Acidity of the Complexes. The higher stability of the dihydrogen complexes of osmium compared to those of its lighter congener ruthenium mirrors a generally observed trend of greater stability against loss of dihydrogen gas for the 5d metals.[35] The fact that the isomers **a** are qualitatively more stable against loss of the dihydrogen ligand than **b** may be the consequence of stronger π-back-bonding from a metal d orbital into the σ^* orbital of the dihydrogen ligand or may reflect a stronger σ Lewis acidity of the complex fragment $[M(CO)L(PPh_3)_2]^+$ in isomers **a**. Since the thiol hydride tautomers, where present, persist longer in solution at higher temperatures, loss of the dihydrogen ligand is probably the main decomposition pathway for complexes **5**−**8**. The structure of **9** suggests that decomposition of the complexes in the presence of excess acid is complete and leads to a rearrangement of the coordination sphere which is totally unrelated to that of complexes **5**−**8**.

The higher relative acidity of the isolable complex **6a** compared to **5a,b** also mirrors a previously noted trend in the series of complexes $[M(H_2)H(L)_2]^+$ (M = Fe, Ru, Os) containing isosteric bistertiary phosphine ligands L.[24] In these complexes the order of acidity of the dihydrogen ligand is 3d > 5d > 4d. This aperiodic trend in the acidity has been attributed to a higher bond dissociation energy ΔH_{BDE} in the ruthenium complexes, reflecting in part the energy required to remove an H atom from the Ru(η^2-H_2) moiety. The ΔH_{BDE} value can be calculated by use of a thermochemical cycle from the experimentally obtained pK_a of the dihydrogen and the first anodic redox potentials $E_{1/2}$ of the parent monohydride complexes.[32,36] The observed acidities here may be a manifestation of the same trend in ΔH_{BDE} values, but the calculation of the ΔH_{BDE} value of the dihydrogen complexes **5a,b** and **6a,b** is not possible for these complexes, since neither the $E_{1/2}$ values of **1**−**4** nor the pK_a values of **5a,b** could be reliably determined.

A comparison of the relative acidities of $[Os(\eta^2\text{-}H_2)(CO)(quS)(PPh_3)_2]^+$ (**8a,b**) and $[Os(\eta^2\text{-}H_2)(CO)(pyS)(PPh_3)_2]^+$ (**6a**) is complicated by the presence of the thiol complexes $[OsH(quSH)(CO)(PPh_3)_2]^+$ (**8c**,**d**) in the reaction mixture, which appear to exchange protons faster than the dihydrogen tautomers. The fact that the tautomeric equilibrium lies on the side of the thiol hydride tautomers does, however, suggest that the dihydrogen complexes are the more acidic species. Thus, it is indeed the relative acidity of the dihydrogen complexes that is probed in the reaction of **6a** with **4a,b** (eq 7). The greater acidity of **6a** compared to the protonation products **8a,b** is counterintuitive, as the higher ν(CO) stretching frequencies of both isomers of **4** compared with **2** suggest that the quinoline-8-thiolate complexes are more oxidizing than the corresponding pyridine-2-thiolate complexes with a lesser extent of π-back-bonding from the metal to the carbonyl ligand. Complexes **4** were therefore expected to form more acidic complexes upon protonation. Just as in the comparison with the ruthenium complexes **5a,b**, a higher bond dissociation energy ΔH_{BDE} of the dihydrogen ligand in **8a,b** may be responsible for the observed lower acidity. As indicated by the carbonyl stretches, π-back-bonding from the metal into empty ligand orbitals is reduced in **8a,b** compared with **6a,b**. This would be consistent with stronger H−H bonding in **8a,b** than in **6a** and thus a higher ΔH_{BDE} and lower acidity of the dihydrogen ligand.

Influence of the Chelate Ligand and the Acid Concentration on Tautomer Ratios and Equilibria of the Protonated Complexes 5−**8.** The subtle electronic differences between the chelating ligands pyridine-2-thiolate and quinoline-8-thiolate that determine the isomer ratios **a,b** in the complexes **1**−**4** also express themselves in the product distributions of the reactions of **1**−**4** with acid. The pyridine-2-thiol/-thiolate complexes favor the dihydrogen tautomers, while the quinoline-8-thiol/-thiolate complexes favor the thiol hydride tautomers. Only one (**5c**) of the 4 possible pyridine-2-thiol hydride complexes **5c,d** and **6c**,**d** is observed, and in only one of the pairs of quinoline type complexes (**8a,c**) is the dihydrogen tautomer dominant under certain conditions.

It is conceivable that the tautomer distributions observed at low temperature represent a kinetic product distribution of the reaction of **1**−**4** with acid. In this

(35) Jessop, P. G.; Morris, R. H. *Coord. Chem. Rev.* **1992**, *121*, 155−284 and references therein.

(36) Tilset, M.; Parker, V. D. *J. Am. Chem. Soc.* **1989**, *111*, 6711−6717.

case the proton would act as a sensitive probe for the site of maximum proton affinity in the monohydride complexes, which then should be correlated to the electron distribution in the frontier orbitals of **1**−**4** determined in the EHMO calculations. We previously reported that, at least for the special case of the tautomer pair **8a,c**, kinetic control of the product distribution seems to be in effect in the presence of excess acid at 193 K.[3] This is expressed by the large jump in the observed tautomer distribution of **8a,c** when the reaction mixture is warmed from 213 to 233 K (Figure 6). The pair **8a,c** shows exceptional behavior, because its tautomer ratio and the temperature response of the tautomeric equilibrium depend on the acid concentration in the mixture (Table 5 and Figures 6 and 7). In the presence of excess acid the dihydrogen tautomer is favored, opposite to the observed trend for the quinoline−thiol/-thiolate complexes.

The reason for this acid concentration dependent behavior may be an ion-pairing phenomenon or the formation of a hydrogen-bonded adduct between free Et_2OH^+ and the protonated complex. The latter would have to stabilize the dihydrogen tautomer relative to the thiol hydride tautomer and would require a *cis* geometry of the two possible hydride and thiol protonation sites. This idea is supported by the presence of two different signals for HBF_4 at 11.6 and 12.6 ppm, indicating that in presence of excess acid, several different free acid moieties exist in solution. Unfortunately, the thermal lability of the complexes severely limits further investigation of this interesting effect.

Under equilibrium conditions the observed temperature-dependent tautomer ratios of **8a,c** and **8b,d** reflect the relative stabilities of the tautomers under the given conditions. Possibly the position of tautomeric equilibria between dihydrogen and hydride complexes with protonated ancillary ligands is correlated with the bond dissociation energy ΔH_{BDE} needed to remove a hydrogen atom from the M(η^2-H_2) unit. It is, however, also possible that secondary effects, such as significantly different solvation energies of the two tautomeric forms, play a decisive role. To test these hypotheses, thermally more stable, isolable systems that display this type of tautomeric equilibrium need to be found that would allow reproducible measurements of the pK_a values of the protonated complexes and the reaction enthalpies and entropies of the equilibrium. Some further insight into the subtle electronic influences that govern such tautomeric equilibria could also be derived from high-level quantum-chemical calculations that are beyond the scope of this report.

Conclusions

We presented here the series of tautomeric dihydrogen $[M(\eta^2\text{-}H_2)(CO)(L)(PPh_3)_2]^+$ and thiol hydride complexes $[MH(CO)(LH)(PPh_3)_2]^+$ (M = Ru, Os; L = pyridine-2-thiolate, quinoline-8-thiolate), which coexist in solution. The osmium complexes $[Os(\eta^2\text{-}H_2)(CO)(quS)(PPh_3)_2]^+$ (**8a,b**) and $[OsH(CO)(quSH)(PPh_3)_2]^+$ (**8c**,**d**) are in a temperature-dependent tautomeric equilibrium with each other. This is the first example of the direct observation of an equilibrium between an acidic dihydrogen complex and a corresponding hydride complex with a protonated ancillary ligand. In at least one case the tautomer distribution at 193 K is kinetically controlled. The stability and tautomer distribution of the protonated complexes depends sensitively on the electronic properties of the chelate ligand L and the metal. With the exception of $[Os(\eta^2\text{-}H_2)(CO)(pyS)(PPh_3)_2]^+$ the protonated complexes are thermally unstable against rapid loss of dihydrogen gas at room temperature and subsequent decomposition. The order of acidity in the protonated complexes $[M(\eta^2\text{-}H_2)(CO)(L)(PPh_3)_2]BF_4$ is Os > Ru and pyS^- > quS^-. The X-ray crystallographic analysis of the decomposition product $[Os(CO)(\mu_2\text{-Spy})(SpyH)(PPh_3)]_2[BF_4]_2$ suggests complete rearrangement of the coordination sphere after loss of the dihydrogen ligand. The complex has an $M_2(\mu_2\text{-Spy})_2$ core with a face-to-face arrangement of the two bridging pyridine-2-thiolate ligands, which is emerging as a common structural motif in these dimers. The isomer distribution of the parent monohydride complexes $MH(CO)(L)(PPh_3)_2$ is thermodynamically controlled and inverts as a function of the chelating thiolate ligand employed. The electron distribution in the free thiolate ligands and the complexes $MH(CO)(L)(PPh_3)_2$ has a decisive influence on the isomer ratios in the monohydride complexes and the tautomer ratios in the corresponding protonated dihydrogen/thiol hydride complexes, respectively. It can be qualitatively interpreted by calculations on the EHMO level.

Experimental Section

Oxygen and water were excluded at all times by the use of a glovebox supplied with purified nitrogen or vacuum lines supplied with purified N_2 or Ar; Ar was used unless otherwise stated. Et_2O and hexanes were dried over and distilled from sodium-benzophenone ketyl. For the acidity studies this was done immediately before use. CH_2Cl_2 was distilled from calcium hydride. Toluene was distilled from sodium. Deuterated solvents were dried over Linde type 4 Å molecular sieves and degassed prior to use. The phosphine ligands were used as purchased from Aldrich, Strem Chemicals, or Digital Specialty Chemicals Ltd. Elemental analyses were performed by Canadian Microanalytical Services. The complexes $MH_2(CO)(PPh_3)_3$ and $MH(CO)(pyS)(PPh_3)_2$ (M = Ru (**1**), Os (**2**)) were prepared as reported in the literature.[12,37] NMR spectra were recorded on Varian Unity 400 (400 MHz for ^{1}H, 162 MHz for ^{31}P), Varian Gemini 200 (200 MHz for ^{1}H), and Varian Gemini 300 (300 MHz for ^{1}H, 120.5 MHz for ^{31}P) spectrometers. All ^{31}P NMR spectra were proton-decoupled, unless stated otherwise. ^{31}P NMR chemical shifts were measured relative to ∼1% $P(OMe)_3$ in C_6D_6 sealed in coaxial capillaries and are reported relative to H_3PO_4 by use of $\delta(P(OMe)_3)$ 140.4 ppm. ^{1}H chemical shifts were measured relative to partially deuterated solvent peaks but are reported relative to tetramethylsilane. In all cases, high-frequency shifts are reported as positive. Variable-temperature T_1 measurements were made at 300 or 400 MHz using the inversion recovery method with calibration of the 90/180° pulse at each temperature. The temperature of the probes was calibrated with the temperature dependence of the chemical shifts of MeOH.[38] Heteronuclear decoupling experiments were carried out at 300 MHz and nOe difference measurements at 400 MHz. IR spectra were recorded on a Nicolet Magna IR 550 interfaced to a 486 personal computer. Extended Hückel calculations were performed on a 486 personal Computer using the CACAO program package.[29] In the X-ray crystal structure determinations all calculations were performed and diagrams created

(37) Peet, W. G.; Gerlach, D. H. *Inorganic Syntheses*; McGraw-Hill: New York, 1975.
(38) van Geet, A. L. *Anal. Chem.* **1970**, *42*, 679−680.

using SHE_LXTL-PC on a 486-66 personal computer.[39] Electrochemical measurements were made on a Princeton Applied Research Model 273 potentiostat/galvanostat (without *iR* compensation) interfaced with a Macintosh SE running Interactive Cyclic Voltammogram Acquisition Program (ICYVAP).[40] All cyclic voltammograms were obtained using an electrochemical cell consisting of a platinum working electrode, tungsten secondary electrode, and silver-wire reference electrode in a Luggin-Haber probe capillary. All measurements were made under Ar gas using 0.2 M NBu_4PF_6 in freshly distilled CH_2Cl_2 as the electrolyte solution. The cyclic voltammograms were collected as two cycles of negative to positive to negative potential sweeps. The applied potential was varied over a 2 V range from −0.6 to +1.4 V.

RuH(CO)(quS)(PPh_3)$_2$ (3a,b). Quinoline-8-thiol hydrochloride (300 mg, 1.5 mmol) was dissolved in a mixture of 5 mL of water and 10 mL of ethanol to give a clear, cherry red solution. This was combined with a solution of $RuH_2(CO)(PPh_3)_3$ (450 mg, 0.5 mmol) in 100 mL of toluene. To the biphasic mixture was added $NaHCO_3$ (500 mg, excess) with stirring, causing the organic phase to turn red immediately due to dissolution of quinoline-8-thiol in the organic phase. The mixture was heated to reflux for 2 h. The solvents were removed completely in vacuo. The red residue was redissolved in CH_2Cl_2 and the solution passed through a short column of basic alumina (2.5 × 10 cm) to remove excess ligand. The column was eluted with two 30 mL portions of CH_2Cl_2, and the combined eluates were concentrated in vacuo to a total volume of about 20 mL. Then, 100 mL of hexanes was layered on top of the deep red solution. After 3 days at −20 °C a bright red, air-stable, microcrystalline solid formed. Filtering, washing with hexanes, and drying in vacuo gave 300 mg of product (0.37 mmol, 74%). The solid was a 1:3 mixture of the isomers **3a** (minor isomer, H *trans* to N) and **3b** (major isomer, H *trans* to S). See Table 2 for NMR and IR spectroscopic data. ^{1}H NMR (300 MHz, $CDCl_3$): δ 6.2−7.6 (m, 30H + 5H, overlapping PPh_3 and quinoline-8-thiolate resonances). Anal. Calcd for $C_{46}H_{37}NOP_2SRu$: C, 67.79; H, 4.58; N, 1.72. Found: C, 67.47; H, 4.59; N, 1.75.

OsH(CO)(quS)(PPh_3)$_2$ (4a,b). $OsH_2(CO)(PPh_3)_3$ (400 mg, 0.3 mmol) was dissolved in 10 mL of toluene. To this solution was added quinoline-8-thiol (90 mg, 0.46 mmol) in 20 mL of toluene. The solution was heated to reflux for 24 h, during which time the color changed from red to a deep purple. The reaction mixture was filtered through Celite and pumped down to dryness. The residue was redisolved in 5 mL of CH_2Cl_2, layered with 25 mL of hexanes, and stored at −20 °C. After 2 days the product (160 mg, 0.18 mmol, 59%) was isolated as a deep red, microcrystalline solid. Concentrating the mother liquor gives a second yield, usually contaminated with free ligand. The solid is a 1:3 mixture of the isomers **4a** (minor isomer, H *trans* to N) and **4b** (major isomer, H *trans* to S). See Table 2 for NMR and IR spectroscopic data. ^{1}H NMR (300 MHz, $CDCl_3$): δ 6.2−7.6 (m, 30H + 5H, overlapping PPh_3 and quinoline-8-thiolate resonances). Anal. Calcd for $C_{46}H_{37}NOOsP_2S$: C, 61.11; H, 4.13; N, 1.55. Found: C, 59.94; H, 4.13; N, 1.61.

EHMO Calculations on pyS$^-$, quS$^-$, and OsH(CO)(pyS)(PH_3)$_2$ (2a*). The geometries of the chelates were obtained from CHEM3D minimized models using the standard parameter file supplied with the program.[41] The geometry of **2a*** was based on the X-ray data for **6a**. It was assumed that the Os−N, Os−S, and Os−C bond distances change little on protonation of the hydride ligand in **2a**. The PPh_3 ligands in **2** were replaced with PH_3 to allow use of the CACAO program package. The Os−H distance was set to the standard bond length of 1.6 Å[34] and the bond positioned at an angle of 90° to the carbonyl ligand in the plane defined by the metal and the chelate.

[Os(η^2-H_2)(CO)(pyS)(PPh_3)$_2$]BF_4 (6a,b). (a) Observation of the Isomeric Mixture in Solution. In a 5 mm NMR tube **2a,b** (30 mg, 0.035 mmol) was dissolved in 1 mL of $CDCl_3$ and 10 μL of HBF_4·Et_2O (excess, 85% in Et_2O) was added, resulting in an immediate color change from yellow to almost colorless. Under 1 atm of argon this solution was stable for several days at room temperature (298 K). The spectrum showed an isomeric mixture of **6a** (major isomer, H *trans* to N) and **6b** (minor isomer, H *trans* to S), reflecting the isomer distribution of the parent monohydride complex **2a,b** (2:1). ^{1}H NMR ($CDCl_3$, 400 MHz): δ −5.70 (br, 2H, Os(η^2-H_2), **6a**), −6.84 (br, 2H, Os(η^2-H_2), **6b**), 5.85, 6.29, 6.72, 7.16 (br, 4H, 2-pyridinethiolate protons), 7.20−8.00 (30 H, phenyl region, **6a**). The corresponding peaks for **6b** are obscured by resonances of **6a**. ^{31}P NMR (300 MHz, CH_2Cl_2): δ 9.07 (s, **6a**), 11.77 (s, **6b**). IR (CH_2Cl_2): ν(CO) 1993 cm^{-1}. The ν(CO) peaks of the isomers are not resolved in the IR spectrum.

(b) Isolation of 6a. **2** (230 mg, 0.27 mmol) was dissolved in 15 mL of CH_2Cl_2, and 70 μL of HBF_4·Et_2O (excess, 85% in Et_2O) was added, causing an immediate color change from yellow to colorless. A 60 mL portion of hexanes was added with stirring and the solution stored at −20 °C for several days. A light yellow precipitate formed, from which slow gas evolution was observed. Filtering and drying in vacuo yields a light yellow solid (230 mg, 0.24 mmol, 90%).[11] ^{1}H and ^{31}P NMR spectra show only the presence of **6a**.

[Os(η^2-HD)(CO)(pyS)(PPh_3)$_2$]BF_4 (6c). Under 1 atm of Ar, **2a,b** (10 mg) was dissolved in 1 mL of $CDCl_3$ and DBF_4 in Et_2O (excess, obtained from the reaction of EtOD with $Et_3O^+BF_4^-$) was added, resulting in an immediate color change from yellow to almost colorless. ^{1}H NMR (400 MHz): δ −5.7 (J(HD) = 21 Hz). The corresponding HD complex of the minor isomer could not be observed.

Protonation of MH(CO)(L)(PPh_3)$_2$ (M = Ru, L = pyS$^-$; M = Ru, Os, L = quS$^-$) with HBF_4 at Low Temperature. VT NMR Studies. In a typical experiment 30 mg (0.035 mmol) of complex was dissolved in 0.6 mL of CD_2Cl_2 under 1 atm of hydrogen gas and transferred to a 5 mm NMR tube fitted with a septum. The sample was cooled to 195 K, and 6 μL of HBF_4·Et_2O (85% in Et_2O; 1 mmol = 173 μL) was added using a microliter syringe. The cold sample was briefly shaken to homogenize the viscous solution and inserted into the NMR spectrometer precooled to 193 K. Spectra were recorded immediately in temperature intervals of 10−20 K up to room temperature or the temperature of complete decomposition, as indicated by the lack of signals in the hydride region in the spectrum and formation of a precipitate.

[Ru(η^2-H_2)(CO)(pyS)(PPh_3)$_2$]BF_4 and [RuH(CO)(pySH)(PPh_3)$_2$]BF_4 (5). The complexes can only be observed at temperatures below 233 K. Above that temperature irreversible loss of H_2 gas and rapid decomposition occurs. ^{1}H NMR (CD_2Cl_2, 300 MHz, 193 K): δ −6.05 (br, 2H, Ru(η^2-H_2), **5a**), −7.30 (br, 2H, Ru(η^2-H_2), **5b**), −13.41 (pseudo t (dd), J(HP^x) = J(HP^y) = 18.6 Hz, 1H, Ru*H*(pySH), **5c**), 5.5−8 (m, 34 H, overlapping signals of pyridine-2-thiolate and PPh_3 protons). ^{31}P NMR (300 MHz, CD_2Cl_2, 193 K): δ 36.24 (s, **5a**), 40.24 (s, **5b**), 40.79 and 49.63 (br, **5c**).

[Ru(η^2-H_2)(CO)(quS)(PPh_3)$_2$]BF_4 and [RuH(CO)(quSH)(PPh_3)$_2$]BF_4 (7). The η^2-H_2 complex of the major isomer **7a** can only be observed for a short period of time at temperatures below 213 K. Even at that temperature irreversible loss of H_2 gas and decomposition occurs. The complexes **7b**−**d** can be observed up to 273 K. Above that temperature decomposition takes place. The peak assignments are based on a ^{1}H-{^{31}P} heteronuclear decoupling experiment. ^{1}H NMR (300 MHz, CD_2Cl_2, 193 K): δ −5.4 (br, 2H, Ru(η^2-H_2), **7b**), −7.5 (br, 2H, Ru(η^2-H_2), **7a**), −8.81 (t, J_{HP} = 17.8 Hz, 1H, Ru*H*(quSH), **7d**), 4.51 (dd, J_{HP} = 21.8, 8.5 Hz, 1H, RuH(quS*H*),

(39) Sheldrick, G. M. SHE_LXTL/PC V5.0, PC program; Siemens Analytical X-ray Instruments, Karlsruhe, West Germany, 1990.

(40) Burrow, T. Interactive Cyclic Voltammogram Acquisition Program (ICYVAP); Apple Macintosh program, unpublished, Toronto, 1994.

(41) CSC CHEM3D, Apple Macintosh Program, Cambridge Scientific Computing, Inc., Cambridge, MA, 1993.

7d), −11.58 (t, J_{HP} = 15.4 Hz, 1H, Ru*H*(quSH), **7c**), 4.35 (dd, J_{HP} = 19.4, 6.7 Hz, 1H, RuH(quS*H*), **7c**) (**7d** partially overlaps with the signal for free H_2 gas at 4.6 ppm), 6.00−8.00 (m, 30H + 6H, signals of PPh_3 and quinoline-8-thiolate/thiol). ^{1}H NMR (300 MHz, CD_2Cl_2, >253 K): δ 4.51 (t, J_{HP} = 10.1 Hz, **7d**), 4.28 (t, J_{HP}= 17.00 Hz, **7c**). ^{31}P NMR (300 MHz, CD_2Cl_2, 193 K): δ 27.20 (s, **7b**), 33.34 (s, **7a**), 55.59 (d, J_{PP} = 248.2, **7d**) and 48.09 (d, J_{PP} = 248 Hz, **7d**), 55.19 (J_{PP} = 247.5, **7c**) and 46.76 (J_{PP} = 246.3 Hz, **7c**), 5.59 (s, $HPPh_3^+$ from start of decomposition).

[Os(η^2-H_2)(CO)(quS)(PPh_3)$_2$]BF_4 and [OsH(CO)(quSH)(PPh_3)$_2$]BF_4 (8). The complexes **8a**−**d** can be observed up to 273 K. Above that temperature decomposition takes place. The peak assignments are in analogy to those made for **7a**−**d**. ^{1}H NMR (300 MHz, CD_2Cl_2, 193 K): δ −3.30 (br, 2H, Os(η^2-H_2), **8b**), −6.3 (br, 2H, Os(η^2-H_2), **8a**), −9.34 (t, J_{HP} = 17.6 Hz, 1H, Os*H*(quSH), **8d**), 5.17 (dd, J_{HP} = 13.2, 6.8 Hz, 1H, OsH(quS*H*), **8d**), −13.04 (t, J_{HP} = 15.9 Hz, 1H, Os*H*(quSH), **8c**), 4.95 (dd, J_{HP} = 21.4, 14.2 Hz, 1H, OsH(quS*H*), **8c**). 6.00−8.00 (m, 30H + 6H, signals of PPh_3 and quinoline-8-thiolate/thiol). ^{1}H (300 MHz, CD_2Cl_2, > 253 K): δ 5.16 (t, J_{HP} = 12.2 Hz, 1H, **8d**), 5.30 (t, J_{HP} = 16.0 Hz, 1H, **8c**). The chemical shift of the thiol protons varies with temperature and acid concentration. ^{31}P NMR (300 MHz, CD_2Cl_2, 193 K) δ: 0.93 (s, **8b**), 8.23 (s, **8a**), 29.12 (d, J_{PP} = 233.7 Hz, **8d**), 21.54 (d, J_{PP} = 233.8 Hz, **8d**); the peaks for **8c** are not resolved and appear as shoulders on the peaks of **8d**. Above 253 K **8d** broadens due to an increased rate of inversion at the sulfur.

Reaction of RuH(CO)(pyS)(PPh_3)$_2$ (1a,b) with [Os(η^2-H_2)(CO)(pyS)(PPh_3)$_2$]BF_4 (6a) at Low Temperature. 1 (20 mg, 0.026 mmol) and **6a** (40 mg, 0.042 mmol, 1.5-fold excess) were each individually dissolved in 2 mL of CH_2Cl_2 and the solutions cooled to 193 K. At this temperature the two solutions were combined in a 10 mm NMR tube, the sample was inserted into the precooled spectrometer (300 MHz), and the spectrum was recorded.

Reaction of OsH(CO)(quS)(PPh_3)$_2$ (4a,b) with [Os(η^2-H_2)(CO)(pyS)(PPh_3)$_2$]BF_4 (6a) at Room Temperature. 4 (15 mg, 0.017 mmol) and **6a** (35 mg, 0.035 mmol, 2-fold excess) were each individually dissolved in 2 mL of CH_2Cl_2 and combined in a 10 mm NMR tube, and the ^{31}P{^{1}H} NMR spectrum was recorded immediately.

[Os(CO)(μ_2-Spy)(SpyH)(PPh_3)]$_2$[BF_4]$_2$ (9). X-ray grade crystals of **9** were obtained by slow diffusion of Et_2O into a solution of **6** in CH_2Cl_2 in the presence of excess HBF_4 and air. The crystals of **9** are slightly soluble only in $CHCl_3$. ^{1}H NMR (400 MHz, $CDCl_3$): δ 13.00 (NH of mercaptopyridinium), 5.70−8.20 (m, signals for PPh_3 and pyridine-2-thiolate). ^{31}P NMR (300 MHz, $CHCl_3$): δ 9.62 (s). IR ($CHCl_3$): ν(CO) 1948 cm^{-1}. FAB-MS (bulk material): calcd for $C_{58}H_{48}N_4O_2Os_2P_2S_4$ *m/e* 1404, obsd $M^{2+} - H^+$ *m/e* 1403.

X-ray Crystal Structure Determination of [Os(CO)(μ_2-Spy)(SpyH)(PPh_3)]$_2$[BF_4]$_2$ (9). A summary of selected crystallographic data is given in Table 7. Data were collected on a Siemens P4 diffractometer using graphite-monochromated Mo Kα radiation (λ = 0.710 73 Å). The intensities of 3 standard reflections measured every 97 reflections showed no decay. The data were corrected for Lorentz and polarization effects and for absorption[42] (minimum and maximum corrections were 0.3264 and 0.7282). Refinement was by full-matrix least squares on F^2 using all data (negative intensities included). Apart from the disordered atoms of the cation, all non-hydrogen atoms were refined with anisotropic thermal parameters. The weighting scheme was $w = 1/[\sigma^2(F_o^2) + (0.0339P)^2]$, where $P = (F_o^2 + 2F_c^2)/3$. Hydrogen atoms were included in calculated positions and treated as riding atoms with isotropic displacement parameters U_{iso} = 0.052 Å^2 for the pyridine-2-thiolate ligands and U_{iso} = 0.055 Å^2 for the phenyl ligands. The dimeric cations have crystallographic 2-fold symmetry. The symmetrically equivalent mercaptopyridinium ligands are conformationally disordered over two sites (with relative occupancies 0.44 and 0.56). The disordered atoms of the cation were refined with isotropic thermal parameters. There are two BF_4^- counterions and two CH_2Cl_2 solvent molecules associated with each dimer molecule. The unique BF_4^- ion was refined as a rigid group which is rotationally disordered (relative occupancies 0.50 and 0.50) about a B−F bond.

(42) Sheldrick, G. M. SHELXA-90, Program for Absorption Correction, PC program; Universität Göttingen, Göttingen, Germany, 1990.

Table 7. Summary of Crystal Data, Details of Intensity Collection, and Least-Squares Refinement Parameters

empirical formula	$C_{58}H_{48}N_4O_2Os_2P_2 \cdot 2[BF_4] \cdot 2[CH_2Cl_2]$
M_r	1747.06
cryst size, mm	0.44 × 0.34 × 0.28
cryst class	monoclinic
space group	*C*2/*c*
temperature, K	173(2)
a, Å	28.287(3)
b, Å	10.1513(14)
c, Å	25.185(3)
β, °	116.578(8)
V, A^3	6467.6(14)
Z	4
D_{calcd} g cm^{-3}	1.794
μ(Mo Kα), cm^{-1}	43.39
F(000)	3408
ω scan width, deg	0.77
range θ collected, deg	2.58−30.00
no. of rflns collected	9600
no. of indep rflns	9426
R_{int}	0.0387
no. of obsd data ($I > 2\sigma(I)$)	5787
R1 ($I > 2\sigma(I)$)	0.0403
wR2 (all data)[a]	0.0862
goodness of fit	0.816
no. of params refined	417
max density in ΔF map, e Å^{-3}	1.339

[a] Definition of *R* indices: $R1 = \Sigma(F_o - F_c)/\Sigma(F_o)$; $wR2 = [\Sigma[w(F_o^2 - F_c^2)^2]/\Sigma[w(F_o^2)^2]]^{1/2}$.

Acknowledgment. We thank Dongmei Wang and Robert J. Angelici (Department of Chemistry, Gilman Hall, Iowa State University) for carrying out the calorimetric titrations and N. Plavac (Department of Chemistry, University of Toronto) for help with the NMR studies. We are grateful to the NSERC and the donors of the Petroleum Research Fund, administered by the American Chemical Society, for research grants and Johnson Matthey PLC for a loan of ruthenium and osmium salts.

Supporting Information Available: X-ray crystal structure information for complex **9,** including tables of atomic coordinates, intramolecular bond lengths and angles, thermal parameters, and hydrogen atom coordinates and an ORTEP plot of the disordered BF_4^- counterion and a CH_2Cl_2 solvent molecule (8 pages). Ordering information is given on any current masthead page.

OM960411H